Aus der Klinik für Kardiologie (CVK)
der Medizinischen Fakultät der Charité – Universitätsmedizin Berlin

DISSERTATION

Network dynamics of coupled mitochondrial oscillators in cardiac cells

zur Erlangung des akademischen Grades
Doctor medicinae (Dr. med.)

vorgelegt der Medizinischen Fakultät der
Charité – Universitätsmedizin Berlin

von

Felix Tobias Kurz

aus *Heidelberg*

Datum der Promotion: 25.10.2013

CONTENTS

Abstract

Inter-mitochondrial coupling in cardiac cells initiates synchronized mitochondrial network behavior under oxidative and metabolic stress. Cellular imbalances in reactive oxygen species (ROS) handling lead to a collapse of inner mitochondrial membrane potential $\Delta\Psi_m$ and ensuing self-sustained periodic $\Delta\Psi_m$ oscillations that are propagated by ROS-induced ROS release. Gaining information about the temporal properties of individual mitochondrial oscillators is essential to comprehend the network's intrinsic spatio-temporal organization. In the present work, signal processing tools have been developed to detect individual mitochondrial tetramethylrhodamine ethyl ester fluorescence oscillations and assess their dynamical properties, using wavelet analysis. Motivated by heterogeneous frequency behavior, mitochondria were sorted according to their frequencies into different mitochondrial clusters with similar frequencies. For the largest cluster, signal analysis of the mitochondrial network showed an inverse relationship between cluster size and cluster frequency as well as between cluster amplitude and cluster size. Cross correlation coefficients between neighboring mitochondria clustered along the myocyte striations were higher than for neighboring mitochondria clustered perpendicularly to striations, thus indicating anisotropic communication between mitochondria. The results suggested that frequency and amplitude modulation of clusters of synchronized mitochondria arise through strong changes in local coupling between neighboring mitochondria.

Therefore, apart from isolated glucose-perfused cardiac cells, the same signal processing tools were applied to uncover similar spatio-temporal mitochondrial cluster properties in myocytes of the intact heart, where myocytes are physiologically connected through gap junctions. Furthermore, given the switch in energy substrate utilization during heart failure, cardiac cells were perfused with metabolic agents other than glucose (pyruvate, lactate and β-hydroxy-butyrate) to reveal substrate-specific spatio-temporal mitochondrial network organization.

Moreover, a stochastic phase model was developed that extends the basic Kuramoto model for a network of coupled oscillators to time-dependent coupling constants and frequencies that drift in time for each mitochondrial oscillator. The model therefore quantifies mitochondrial coupling in the pathophysiological regime via substrate-specific coupling constants. Coupling was found to be stronger for cluster mitochondria than for non-cluster mitochondria and to be stronger for higher oscillation

frequencies. The findings indicate a strong mutual influence of ROS formation and metabolic pathway alterations on mitochondrial spatio-temporal organization.

Abstrakt

Unter Einwirkung von oxidativem und metabolischem Stress kann die Kopplung zwischen Mitochondrien in Herzzellen ein synchronisiertes Verhalten des mitochondrialen Netzwerkes initiieren. Zelluläre Ungleichgewichte im Umgang der Zelle mit reaktiven Sauerstoffspezies (ROS) führen zu einem Kollaps des inneren mitochondrialen Membranpotentials $\Delta\Psi_m$ und die folgenden sich selbst-erhaltenden periodischen $\Delta\Psi_m$ Oszillationen werden über ROS-induzierte ROS-Freisetzung propagiert. Es ist für das Verständnis der intrinsischen spatio-temporalen Organisation des mitochondrialen Netzwerkes essenziell, Informationen über die temporalen Eigenschaften der individuellen mitochondrialen Oszillatoren zu gewinnen. In der vorliegenden Arbeit sind Methoden zur Signalprozessierung entwickelt worden, um individuelle mitochondriale Tetramethylrhodamineethylester-Fluoreszenz-Oszillationen zu detektieren und, mit der Hilfe von Wavelet-Analyse, deren dynamischen Eigenschaften zu beurteilen. Heterogene Frequenzeigenschaften von Mitochondrien dienten als Motivation, Mitochondrien nach ihren Frequenzen in verschiedene mitochondriale Cluster mit ähnlichen Frequenzen einzuteilen. Für das größte solche Cluster zeigte die Signalanalyse des mitochondrialen Netzwerks eine inverse Beziehung zwischen Cluster-Größe und Cluster-Frequenz und ebenso zwischen Cluster-Amplitude und Cluster-Größe. Höhere Kreuzkorrelation-Koeffizienten zwischen benachbarten Mitochondrien, die entlang der Streifung der Herzzelle angehäuft sind, als zwischen senkrecht dazu angehäuften Mitochondrien, weisen auf eine anisotrope Kommunikation zwischen Mitochondrien hin. Die Resultate ließen vermuten, dass Modulation von Frequenz und Amplitude der Cluster von synchronisierten Mitochondrien anhand von starken Veränderungen der lokalen Kopplung zwischen benachbarten Mitochondrien entstehen.

Deshalb wurde dieselbe Art der Signalprozessierung neben isolierten Glukose-perfundierten Herzzellen auch für Verbände von Herzzellen angewandt, die physiologisch über gap junctions miteinander verbunden sind. Es konnten ähnliche spatio-temporale Eigenschaften der mitochondrialen Cluster festgestellt werden. Da während Herzinsuffizienz ein Wechsel in der energetischen Substratausnutzung stattfindet, wurden die Herzzellen zudem mit, neben Glukose, weiteren metabolisch relevanten Lösungen perfundiert (Pyruvat, Laktat, β-Hydroxybutyrat). Hier zeigte sich eine substrat-spezifische spatio-temporale Organisation des mitochondrialen

Netzwerks.

Weiter wurde ein stochastisches Phasenmodell entwickelt, welches das grundlegende Kuramoto-Modell eines Netzwerks von gekoppelten Oszillatoren auf für jeden mitochondrialen Oszillator zeitabhängige Kopplungskonstanten und Frequenzen erweitert, die im zeitlichen Verlauf von ihrer Ausgangsfrequenz abdriften. Das Modell quantifiziert so mitochondriale Kopplung im pathophysiologischen Regime über substrat-spezifische Kopplungskonstanten. Die Kopplung zwischen Cluster-Mitochondrien wurde als stärker als zwischen Nicht-Cluster-Mitochondrien festgestellt. Außerdem war die mitochondriale Kopplung stärker bei höheren Oszillationsfrequenzen. Die Ergebnisse verdeutlichen den gemeinsamen Einfluss von ROS-Formierung und Veränderungen der metabolischen Übertragungswege auf die mitochondriale spatio-temporale Organisation.

I Introduction

In mammalian organisms, mitochondria are essential power-supplying organelles that are surrounded by two lipid bilayers which separate four distinct compartments: the outer membrane, intermembrane space, inner membrane and the matrix [1]. The inner bilayer is convoluted such that a large number of infoldings called cristae are formed [1,2] which accommodate the complexes of the electron transport chain and adenosine-5'-triphosphate (ATP) synthase [2].

1.1 Mitochondrial pathway regulation

No other cell organelle possesses greater structural or functional diversity: mitochondria are involved in numerous pathways, ranging from synthesis of amino-acids, steroids and heme to β-oxidation of fatty acids, oxidative phosphorylation, control of calcium signaling and apoptosis-programmed cell death [1,3]. Mitochondrial oxidative phosphorylation and electron transport chain appear fully understood [4], nevertheless, there are two different explanatory mechanisms that have been proposed to form the basis of mitochondrial pathway regulation. The classical mechanism supports the hypothesis that regulation of adenosine diphosphate (ADP) and inorganic phosphate (Pi) controls cardiac ATP metabolism [5]. However, recent studies provided evidence that measured ADP/Pi concentrations did not change for large cardiac ATP consumption [6,7]. The second mechanism proposes mitochondrial pathway regulation through cytosolic calcium [8,9] (Figure 1.1). Modulatory function may be attributed to both regulatory mechanisms with ADP/Pi being more involved in the regulation of oxidative phosphorylation and cytosolic calcium in the regulation of Krebs cycle dehydrogenases [10].

1.2 Mitochondria in cardiac cells

Constant ATP generation in cardiac myocytes is required to suffice the enormous energy that is consumed by the working human heart: to keep systemic and pulmonary blood pressure at working level through normal contraction and to fuel basic metabolism, cardiac cells synthesize approximately 30kg of ATP from ADP each day [11]. Since almost all ATP is produced by cardiac mitochondria, except for small amounts of cytosolic ATP generation, mitochondria are densely packed in cardiomyocytes, accounting for about 35% of their volume [12]. They are organized in a highly ordered network with lattice-like morphological manifestation, mostly arranged parallel to the

long axis of the cardiac myocyte. Mitochondrial location is therefore closely associated with the sarcoplasmic reticulum (SR) that provides the possibility of easy intracellular ATP distribution [13]. ATP is needed for calcium reuptake via the SR calcium ATPase (SERCA) after sarcomeric contraction [14]. Further excess calcium is exported through the sodium-calcium-exchanger [15] and the plasmalemmal calcium ATPase [16,17] to eventually terminate contraction [18]. Mitochondria can sense SR cytosolic calcium release as a sign of increased need of ATP production [19].

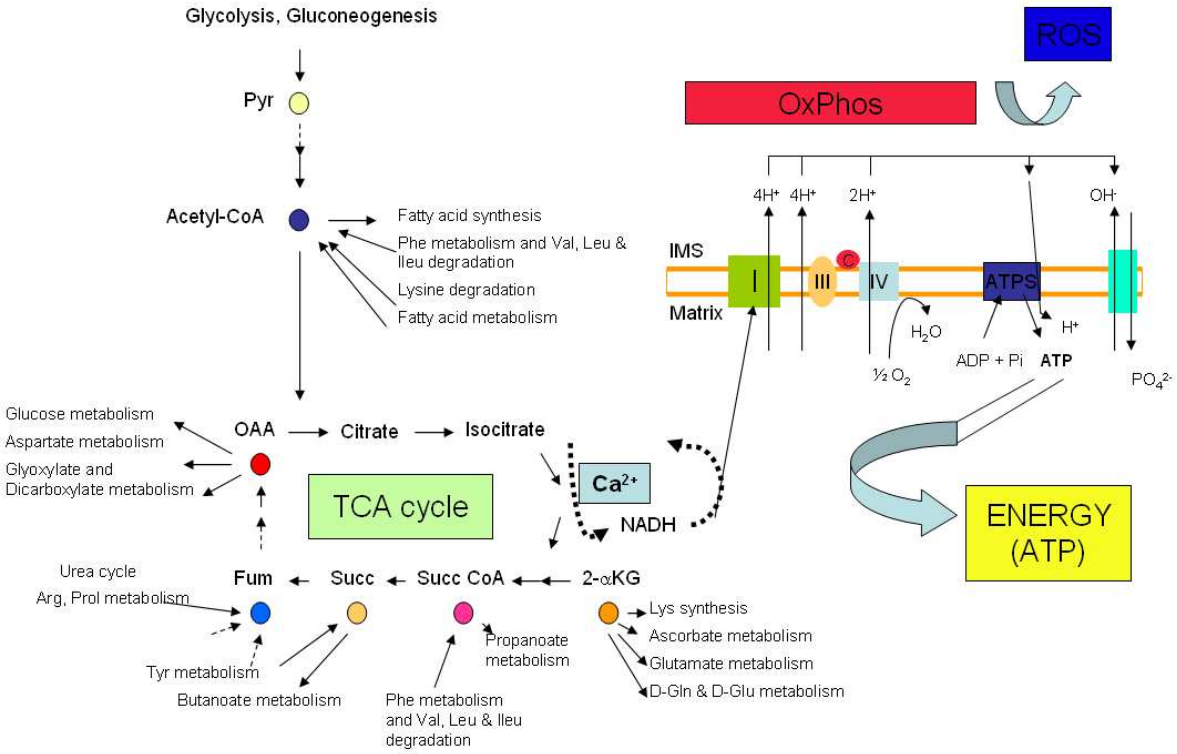

Figure 1.1 Schematic view of mitochondrial metabolism. Within the cellular network, the tricarboxylic acid cycle (TCA cycle) links mitochondria with multiple other metabolic pathways, exemplifying their role as metabolic hubs in cellular metabolism. Pyruvate dehydrogenase and two of the main dehydrogenases that catalyze the conversion of isocitrate and 2-α-ketoglutarate (2-αKG) are activated by calcium [10]. Oxidative phosphorylation (OxPhos) is responsible for production of reactive oxygen species (ROS) at the level of complex I or III and ATP through ATP synthase (ATPS). Further abbreviations: ADP = adenosine diphosphate, Arg = Arginine, ATP = adenosine triphosphate, OAA = oxaloacetate, C = cytochrome C, CoA = Coenzyme A, Fum = fumarate, Gln = glutamine, Glu = glutamate, Ileu = isoleucine, IMS = inner membrane space, Leu = leucine, Lys = lysine, Phe = phenylalanine, Prol = proline, Pyr = pyruvate, Succ = succinate, Tyr = tyrosine, Val = valine. (This diagram has been slightly modified from its original version in Aon et al [70]).

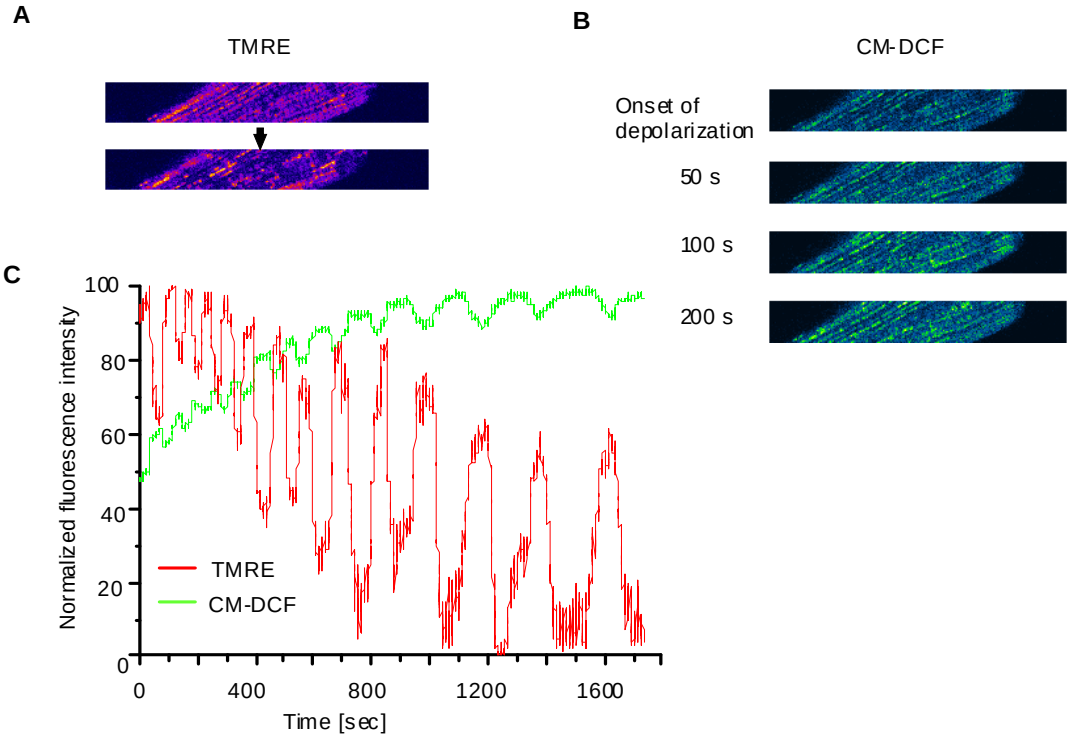

Figure 1.2 Mitochondrial inner membrane potential oscillations and concomitant increase in ROS density. (A) TMRE intensity image of a cardiomyocyte before onset of $\Delta\Psi_m$ depolarization (TMRE intensity scaled from blue to white) and at first $\Delta\Psi_m$ depolarization. (B) Reactive oxygen species (ROS)-sensitive fluorescent probe 5-(and-6)-chloromethyl-2,7-dichlorodihydrofluorescein diacetate (CM-DCF) signal, scaled from blue (reduced) to yellow (oxidized), for different time points after onset of $\Delta\Psi_m$ depolarization. (C) Time course of spontaneous $\Delta\Psi_m$ depolarizations for TMRE and CM-DCF intensity signals. Beginning of TMRE repolarizations coincides with a slight decrease in CM-DCF fluorescence due to increased ROS scavenging in the intermembrane space and deactivation of inner membrane anion channels (IMAC; see also Figure 1.3).

1.3 Mitochondrial inner membrane oscillations

Mitochondrial oxidative phosphorylation depends on the vectorial arrangement of ion transporters, pumps and channels in a selectively permeable inner membrane that enables highly regulated adjustments of mitochondrial volume, inner mitochondrial membrane potential and redox potential [20] to fine tune the balance of energy supply and demand. Mitochondria in the cardiac myocyte under the influence of substrate deprivation or oxidative stress may undergo a transition into a pathophysiological state

where their inner membrane potential $\Delta\Psi_m$ depolarizes and oscillates [20,21,22] (Figure 1.2A,C).

First descriptions of this phenomenon date back to 1982 when Berns et al. were using focal laser excitation to induce spontaneous transient depolarization-repolarization cycles of $\Delta\Psi_m$ in quiescent cardiac myocytes [23]. Similar behavior was observed for mitochondrial depolarizations in cultured neurons [24], in smooth muscle cells [25] and in individual isolated mitochondria [26].

Eventually, when O'Rourke et al. [27] examined guinea pig cardiomyocytes under substrate deprivation, they found cyclical activation of ATP-sensitive potassium currents as well as related low frequency oscillations in action potential duration and excitation-contraction coupling. Oscillatory behavior was associated with oxidation and reduction of the intracellular nicotinamide adenine dinucleotide (NADH) concentration. At first, the mechanism was believed to be modulated by alterations in the glucose metabolism, thus suggesting rhythm generation at the level of glycolysis. However, subsequent studies found the association of these oscillations with mitochondrial flavoprotein redox transients and waves of mitochondrial membrane potential depolarization [28]. The reports implied a mitochondrial origin of the observed phenomena and it was eventually discovered that oscillations could be reproduced reliably by laser-induced depolarization of just a small number of mitochondria [29].

Mitochondrial ionic oscillations have already been observed for isolated liver or heart mitochondria [30] where it was found that ion concentrations of hydrogen (H^+) and potassium (K^+) in the cytosol were sinusoidally oscillating through induction by valinomycin in the presence of oxygen [31]. The oscillations were found to be damped in isolated mitochondria by regulation of external pH, the K^+/H^+ ratio, ADP and the mitochondrial inner membrane's F_1F_0ATPase. Furthermore, it had been shown that adding strontium (Sr^{2+}) to mitochondrial suspensions served as a trigger of oscillations in fluxes of divalent ions across mitochondrial membranes and that these oscillations were dependent on the amount of added Sr^{2+} (see [32]).

The notion that oscillations depended on the fluorescence dye was of considerable significance since it indicated the dependence on photosensitization. It could be demonstrated by Zorov and Sollot [33,34] that application of a focal laser pulse produces fluorescence excitation that could generate enough free radicals to produce mitochondrial depolarization, thus suggesting involvement of reactive oxygen species

(ROS) in the form of mitochondrial ROS-induced ROS release in cardiac myocytes (cf. Figures 1.2B-C, 1.3).

Experimentally, $\Delta\Psi_m$ depolarizations have been observed in small clusters of mitochondria in a synchronized large cluster spanning the whole cell [29] or as waves of mitochondrial $\Delta\Psi_m$ depolarizations surpassing intercalated discs between cardiac cells [28].

$\Delta\Psi_m$ can be monitored with the fluorescent dye tetramethylrhodamine ethyl ester (TMRE) [29]. TMRE is an indicator dye that consists of lipophilic cations which are accumulated by mitochondria in proportion to $\Delta\Psi_m$ [35], i.e. TMRE intensity reduces for depolarization of $\Delta\Psi_m$.

1.4 ROS generation and ROS-induced ROS release

Generally, stress-induced imbalance between ROS generation and ROS scavenging capacity in a significant proportion of the mitochondrial network [29] is thought to destabilize $\Delta\Psi_m$ beyond a critical point into a state of ROS-induced ROS release (RIRR). Increased ROS overflow exceeding a threshold level results in the appearance of a spanning cluster of mitochondria oscillating in apparent synchrony throughout the cell, as the mitochondrial network locks into a low-frequency, high-amplitude oscillatory mode [22,36]. Inhibitors of mitochondrial respiration were used to indicate the mechanisms of mitochondrial ROS production [20,29]: it was observed that complex III-derived ROS production serves as the main source of ROS in intact cells. In contrast, ROS generation in complex I appeared to be favored at high $\Delta\Psi_m$ and highly reduced redox potentials, a state usually found for inhibition of mitochondrial respiration. Inhibiting the electron transport chain with cyanide or through inhibition of F_1F_0ATPase with oligomycin provided experimental evidence that mitochondrial electron transport is necessary for ROS production [29].

Depolarization events have been shown to be inhibited by ligands of the mitochondrial benzodiazepine receptor and not by inhibitors of mitochondrial permeability transition pores (mPTP) [37], therefore supporting the assumptions of underlying mechanisms of mitochondrial RIRR and opening of mitochondrial inner membrane anion channels (IMAC) [20,29,38] (Figure 1.3). In fact, it has been found that mitochondrial $\Delta\Psi_m$ depolarizations were induced by FGIN-1-27 (a selective agonist of

the peripheral mitochondrial benzodiazepine receptor (mBzR)), thus implying the modulation of IMAC through mBzR [20]. However, cyclosporin A, an inhibitor of mPTP has been found in other experiments to suppress laser-induced $\Delta\Psi_m$ oscillations and $\Delta\Psi_m$ depolarization waves [34,39], thus suggesting a link between mPTP openings and responses from triggering of RIRR (cf. Figure 1.3).

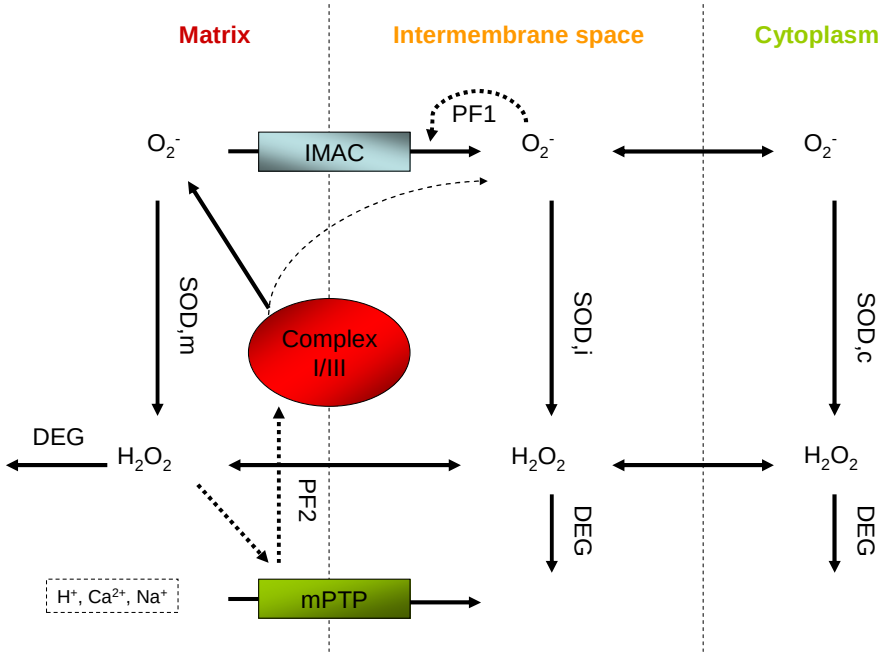

Figure 1.3 Schematic diagram of mitochondrial ROS-induced ROS release models. Superoxide (O_2^-) is produced by complexes I and III and released in the mitochondrial matrix from where it can only exit to the intermembrane space (IS) through IMAC, apart from minor amounts directly exiting complex III (dashed arrow originating from complex III). In matrix, IS and cytoplasm, superoxide dismutases (SOD) convert O_2^- to H_2O_2, which freely diffuses between the three compartments. H_2O_2 is degraded by peroxidases (e.g. glutathione peroxidase; DEG), thereby oxidizing cofactors (e.g. glutathione to glutathione disulfide) [1,10]. O_2^- in IS further activates IMAC for critical ROS densities in the matrix, thus forming a positive feedback loop (PF1) and eventually depolarizing $\Delta\Psi_m$ [29,72]. Ensuing stimulation of SOD activity beyond a critical threshold deactivates IMAC and therefore allows electron transport to restore $\Delta\Psi_m$. In some models [74,75], mPTP opening can be activated by products from H_2O_2-initiated redox processes, e.g. hydroxyl radicals or an oxidized lipid, which leads to temporarily accelerated O2-production in complexes I and III, hence further openings of mPTP in a positive feedback loop (PF2). (This diagram has been slightly modified from its original version in Yang et al [75])

1.5 Mitochondrial morphology, dynamics and morphodynamics

Mitochondrial collective behavior in cardiac myocytes is influenced by mitochondria with different static (morphology and biochemical properties) and dynamic characteristics. For instance, mitochondria in intermyofibrillar locations are morphologically distinct from those in subsarcolemmal or perinuclear regions [40,41]. In fact, mitochondrial morphometric diversity in popular belief is linked to the etymology of the word “mitochondrion” as has been pointed out recently [4]. Here, the word is derived from the Greek words “mitos” (thread) and “khondros” (grain). But the term “mitochondria” was first used by Carl Benda who misleadingly took the Greek word “chondros” (cartilage) to label microscopically observed intracellular organelles that seemed to serve as structures supporting the cell’s shape and size [42].

Mitochondrial static heterogeneity is said to result in different mitochondrial functionalities [43,44]; e.g., mitochondrial function has been found to be prone to alterations through coupling to the L-type calcium channel, assisted by movement of the cytoskeleton [45].

Dynamic heterogeneity is especially significant under metabolic [28] or oxidative stress where small changes in the mitochondrial network organization can inscrease in scale to whole-myocyte and even whole-organ level, potentially contributing to the generation of fatal ventricular arrhythmias [36,46,47,48].

As a matter of fact, cardiac myocytes that are subject to several minutes of ischemia show a severe drop in their action potentials with the onset of $\Delta\Psi_m$ depolarization, thus rendering the cell unexcitable [29] and, upon reperfusion, lead to persistent ventricular tachycardia or even fibrillation [38]. This effect could be prevented successfully with the mBzR antagonist 4'-chlorodiazepam [47]. In contrast, blocking mPTP via cyclosporin A had no effect on ensuing post-ischemic arrhythmias [38,47], thus supporting the idea of a link between IMAC opening and $\Delta\Psi_m$ depolarization. Concomitant activation of sarcolemmal potassium channels creates spatial and likely temporal heterogeneity of cardiac action potentials which can lead to ventricular re-entry [29]. This should not be confused with conduction blocks due to closure of gap junctions between ventricular myocytes where annihilation of a wave of depolarization can be countered with an increase in voltage at the wave front [49].

Ultrastructural changes of mitochondrial morphology from “condensed” to “orthodox” conformations for high (state 3) to low (state 4) respiration rates, respectively,

are well-known [50] and recent studies suggested that specific proteins mediate mitochondrial morphodynamics: it could be demonstrated that dynamin-related proteins mitofusin-1, mitofusin-2 and OPA1 were associated with modulation of fusion and fission events that remodel the structure of mitochondrial inner membranes [51,52] or mitochondrial networks [53,54]. Mitochondrial morphodynamics hence affects proteins that mediate fusion and fission processes, but also influences cellular energetics or calcium levels [55,56] and, through disruption of cytoskeletal architecture, alters mitochondrial mobility [57].

1.6 Complex networks of coupled oscillators

Complex biological systems are often characterized by heterogeneous regulatory mechanisms and nonlinear behavior; therefore, to obtain spatial and temporal organization, living systems use biochemical rhythms that aim to achieve internal coordination [58,59,60,61]. In many disparate examples of physically and chemically coupled oscillators, synchronization of the system arises from an initial nucleus of (spontaneously) synchronized oscillators that integrate neighboring oscillators, therefore increasing the size and signal amplitude of the initial oscillatory nucleus [62,63,64,65]. When the cluster size passes a critical threshold, the whole network spontaneously self-organizes into a new state in a process resembling a phase transition – in the case of mitochondrial oscillators this transition corresponds to the change from the physiological to the pathophysiological regime of the mitochondrial network. Aon et al. [36] found that this global phase transition occurs at a percolation threshold of the mitochondrial network, and further demonstrated that this global behavior obeys fractal, self-similar dynamics [20,22,59] with no inherent characteristic frequency, but rather displays a broad range of frequencies occurring over multiple time scales.

In complex networks, percolation theory provides a probabilistic model to describe collective dynamics of connected network components [66]. Since criticality occurs at about 60% of mitochondria that have ROS levels at or near threshold of synchronized $\Delta\Psi_m$ depolarization, this number is almost equal to the theoretical prediction for lattice-like networks (pc=0.59) [21,36] (Figure 1.4). Percolation theory states that, at percolation threshold, the mitochondrial network is highly susceptible to small perturbations that can lead to a transition into global limit cycle oscillations [36]. However, these considerations apply to regular networks with strict nearest-neighbor

constellations and vary significantly for small changes in the topological alignment of network constituents [67].

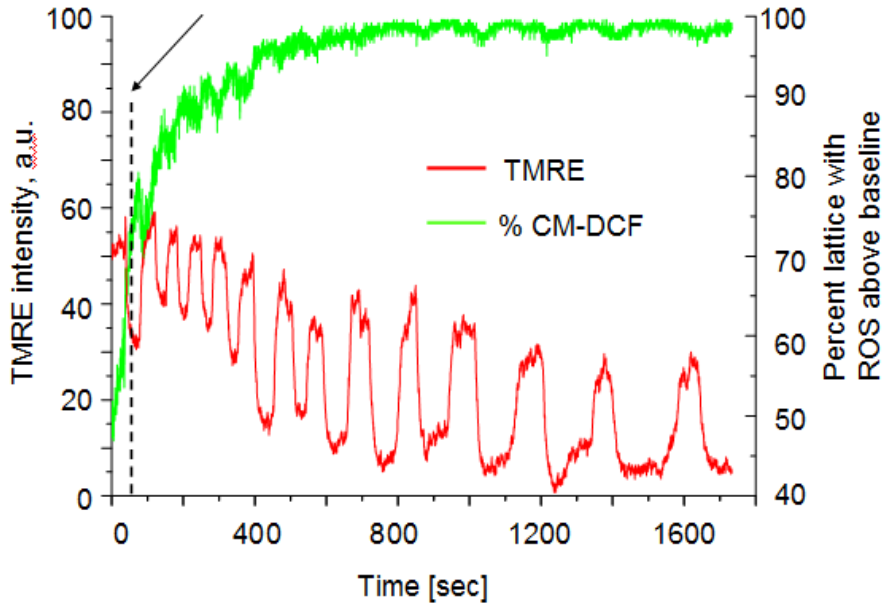

Figure 1.4 Mitochondrial criticality at the percolation threshold. Time course of spontaneous $\Delta\Psi_m$ depolarization for TMRE (red) (indicated by the arrow) and ensuing development of the mitochondrial spanning cluster as ROS density grows. The mitochondrial network reaches criticality when about 50-60% of the mitochondria have CM-DCF fluorescence levels above baseline (green), roughly corresponding to the expected theoretical percolation threshold (pc = 0.59).

Scale-free systems share similar characteristics in their frequency-amplitude relationships on all scales in a time series. For a large network of oscillators this means that formation of new connections between network constituents depends on the number of existing connections for each network node. Specifically, a new connection favors a node with a probability that depends on the number of connections that are already attached to it [68], an effect otherwise known as the “Matthew effect” [69]. The observation that mitochondrial networks follow scale-free dynamics suggested that mitochondrial signal fluctuations are not random excursions but rather an indication of weak inter-mitochondrial coupling by low levels of mitochondrial ROS in the physiological state [70].

1.7 Modeling mitochondrial network behavior

Recently, several computational models of mitochondrial networks have been

proposed to describe mitochondrial network dynamics (see [71] for a detailed review). For instance, Cortassa et al. developed a mathematical model that simulates physiological behavior in ventricular myocytes using ordinary differential equations for the time rate of change of matrix concentrations of calcium, NADH, ADP and Krebs cycle intermediates as well as $\Delta\Psi_m$ [8]. The model correctly reproduced mitochondrial bioenergetics, calcium dynamics and mitochondrial respiration. More recently, the model incorporated IMAC-mediated mitochondrial RIRR [72] to generate $\Delta\Psi_m$ limit cycle oscillations and further diffusion dynamics of ROS [73] (cf. Figure 1.3). This model reproduces network dynamics that match theoretical reasoning of synchronization theories in that it can show that synchronized clusters of mitochondria can entrain mitochondria that would otherwise be displaying stable dynamics [73].

Other models proposed mPTP-mediated RIRR [34,74] or both mPTP-mediated and IMAC-mediated RIRR [75] (Figure 1.3). Also, an agent-based model of mitochondrial network excitability has been developed that determines the probabilities of a network transition to a subsequent state at every step and elucidates that the ROS messenger molecule superoxide can be switched to hydrogen peroxide for increased distances between neighboring mitochondria, hence efficiently blocking RIRR through cytosolic glutathione peroxidase 1 [76].

1.8 The Kuramoto model

Multi-agent systems with self-synchronizing behavior for weakly coupled non-linear oscillators with arbitrary frequencies have been studied extensively over the past decades [62,63,77]. Specifically, the Kuramoto model and subsequent altered versions of it have been applied to many different contexts in circadian biology as well as other biological, physical and chemical systems (reviewed in detail in [63,77]). Briefly, the Kuramoto model relies on the idea that several oscillators can interact in a way such that the individual oscillator's properties change in order to achieve a global behavior for the interconnected system. It assumes nearly identical and weakly coupled limit-cycle oscillators that have intrinsic natural frequencies drawn from a normal distribution around some mean frequency [77]. The Kuramoto model seems mathematically simple but requires complex analytical solutions [63]. Recent studies proposed an extension of the Kuramoto model for biomolecular oscillators that drive synchronized circadian network behavior through mitochondrial intrinsic frequencies that drift in time [78,79].

These frequencies can be described by Ornstein-Uhlenbeck dynamics, a non-linear mathematical formulation for processes that tend to drift towards their long-term mean [80].

Kuramoto models describe phase dynamics through a sinusoidal phase coupling term with a time-independent coupling constant [77]. However, for cardiac myocytes, static and dynamic mitochondrial heterogeneity suggests dynamic mitochondrial coupling as well.

In this work, it will be shown that individual mitochondrial oscillators are subject to dynamically changing frequencies. Using Ornstein-Uhlenbeck frequencies for individual mitochondrial oscillators, this provided motivation to directly quantify time-dependent inter-mitochondrial coupling through observation of individual mitochondrial phase dynamics.

1.9 Motivation and outline

So far, methods to examine mitochondrial network dynamics were based on power spectral analysis and relative dispersional analysis [20,21,22,36] of mesh components of lattice-like grids, with mesh sizes of mitochondrial magnitude that have been superimposed on the cardiac myocyte. This is only in part an accurate method since first, these grids assume the mitochondrial network to be even, symmetrical and non-changing in time. And second, movement of the myocyte during cell recording and therefore movement of the mitochondrial network cannot be taken into account, i.e. the myocyte is assumed to be fixed in one place during the whole recording. Taken together, these assumptions cannot completely cover the complex morphological changes of the mitochondrial network. They only suffice for recordings with a short period of time in which the myocyte does not move and only for a mitochondrial network where the network's physical topology comes close to that of an ideal symmetrical two-dimensional lattice. Therefore, in the present work, a novel method for detecting and characterizing single mitochondrial $\Delta\Psi_m$ oscillations is derived and it will be demonstrated that oscillating mitochondria exhibit dynamically changing frequencies.

The observation that oscillating mitochondria may be spatially organized during myocyte-wide synchronized oscillations supported the hypothesis that individual mitochondria within a cluster might oscillate at the same frequency, and therefore gave rise to the idea of examining whether the oscillation frequency of individual mitochondria

influences the size and amplitude of the mitochondrial cluster oscillations and vice versa. It will be shown how to determine a mitochondrion's cluster affiliation to a cluster of mitochondria with similar frequencies for each sampling point of the recording. Such a frequency cluster should not be thought of as a morphologically connected cluster but rather as a cluster with mitochondria that share similar conditions for their inner membrane potential. While only considering those oscillating mitochondria that belong to the largest frequency cluster, the findings reveal significant correlations between mean mitochondrial cluster frequency and mitochondrial cluster size as well as between mitochondrial cluster amplitude and mitochondrial cluster size, indicating the strong influence of individual mitochondrial oscillators on the spatio-temporal organization and formation of mitochondrial clusters.

In addition, it will be demonstrated (by comparing cross-correlating TMRE fluorescence signals of neighboring mitochondria) that there is a distinctly stronger coupling between neighbors aligned along cardiomyocyte striae than otherwise. Also, mitochondrial criticality is qualitatively studied with an isochronal map at the onset of synchronized TMRE oscillations.

Moreover, given the switch in energy substrate utilization during heart failure [81], the aforementioned signal processing tools will be applied to isolated cardiomyocytes that are perfused with metabolic agents other than glucose (pyruvate, lactate and β-hydroxy-butyrate). In fact, an increase of glycolysis or β-oxidation products is thought to lead, via degradation to acetyl-CoA, to augmented NADH production in the Krebs cycle and hence increase the amount of superoxide radicals provided by the mitochondrial respiratory chain [82], therefore influencing RIRR and mitochondrial network synchronization.

Also, since the induction of synchronization had already been demonstrated for mitochondria in connected cells of the intact heart [83], wavelet-based mitochondrial network analysis will be applied to ensembles of ventricular myocytes in tissue slices of the intact heart where inter-cellular connections through gap junctions render the cells exposed to altered physiological conditions.

Finally, a stochastic model based on the Kuramoto model for coupled oscillators will be introduced that extends the basic Kuramoto model to individual time-dependent coupling constants for each mitochondrial oscillator and that will be used to study inter-mitochondrial coupling characteristics.

The findings will reveal significant correlations between mitochondrial cluster size

and cluster frequency for connected cells in tissue slices of the intact heart and those with substrate-perfusion as demonstrated for isolated glucose-perfused cardiac myocytes. In addition, stochastic modeling across substrates will provide insight into the mitochondrial network's coupling topology and its relation to mitochondrial cluster organization under different metabolic conditions.

II Methods

2.1 Experimental data

All experiments were conducted on freshly isolated adult guinea pig ventricular myocytes according to already established experimental protocols [22,27,29] that will be briefly explained in the following three sections 2.1.1-2.1.3. The experiments were conducted in accordance with the Guide for the Care and Use of Laboratory Animals (NIH, No. 85-23, 1996).

2.1.1 *Isolated myocytes*

Adult guinea pigs (300 g) were anesthetized with 260 mg pentobarbital and 1000 units of heparin sodium (i.p.). The hearts were excised and subjected to the procedure of isolation of ventricular myocytes by enzymatic dispersion [27,84]. After isolation, cells were stored briefly in a high potassium solution (in mM: 120 potassium glutamate, 25 KCl, 1 $MgCl_2$, 10 HEPES, 1 EGTA, pH 7.2 with KOH) and either used immediately or transferred to Dulbecco's Modification of Eagle's Medium (10-013 DMEM, Mediatech, Inc. Virginia) in laminin-coated petri dishes in a 95% O_2, 5% CO_2 incubator at 37°C for at least 2 h before imaging and used within 6-8 hours of isolation. Experimental recordings started after exchange of the DMEM with Tyrode's solution containing (in mM): 140 NaCl, 5 KCl, 1 $MgCl_2$, 10 HEPES, 1 $CaCl_2$, pH 7.4 (adjusted with NaOH), supplemented with 10 mM glucose, β-hydroxy-butyrate, lactate or pyruvate, respectively. The dish containing the cardiomyocytes was equilibrated at 37 °C with unrestricted access to atmospheric oxygen on the stage of a Nikon E600FN upright microscope. The isolation technique yields calcium-tolerant, quiescent myocytes [85]. Substrate deprivation had no untoward effects on the appearance of the myocytes; cells remained rod-shaped with clearly defined striations.

2.1.2 *Whole heart myocytes*

Excised hearts were retrogradely perfused with an oxygenated (100% O_2) modified Tyrode's solution (138 mM NaCl, 4 mM KCl, 0.5 mM $CaCl_2$, 1 mM $MgCl_2$, 0.33 mM NaH_2PO_4, 10 mM glucose, 10 mM HEPES pH 7.4) containing butanedione monoxime (20 mM) to suppress contraction [86]. A custom-built chamber was used to minimize pulsatile motion artifacts and imaging focused on epicardial regions located near (within 5 mm of) the left anterior descending coronary artery [83].

2.1.3 *Fluorescent probes for two-photon laser scanning microscopy and image acquisition*

The cationic potentiometric fluorescent dye tetramethylrhodamine ethyl ester (TMRE) was used to monitor the mitochondrial inner membrane potential $\Delta\Psi_m$. The large potential gradient across $\Delta\Psi_m$ results in an accumulation of TMRE within the matrix compartment according to its Nernst potential [24].

Images were recorded with a two-photon laser-scanning microscope (Bio-Rad MRC-1024MP) with an excitation at 740 nm (Tsunami Ti:Sa laser, Spectra-Physics) and an emission band at 605 ± 45nm.

Light-induced mitochondrial depolarization was applied in a small cytoplasmic volume by zooming the laser beam in on a 20 x 20-pixel (8.7 x 8.7 µm square, < 1 µm focal depth) region of the cell. Because the total scan duration was the same as that used for full frame imaging, the laser dwell time in a given cell volume during a flash is ~655 times the normal. This caused the local generation of ROS because of direct interaction with molecular oxygen to promote triplet state excitation of local fluorophores [26]. Local photon-induced ROS elaboration, reinforced by the restricted irreversible depolarization of $\Delta\Psi_m$, made it possible to perturb a small region of the myocyte in order to look for propagating effects.

2.2 Individual mitochondrial TMRE signals

2.2.1 *Formulation and application of mitochondrial grid*

Qualitatively, for each myocyte, in a stack of TMRE fluorescent images recorded at a rate of dt, the onset of overall TMRE oscillations was identified as the first image with a 10% TMRE intensity loss relative to the mean TMRE intensity averaged over all previous images. Subsequent images were then divided into equally sized intervals consisting of n images with n taken such that $n \cdot dt$ was smaller or equal to the smallest period of all TMRE oscillations.

Thereafter, an average image from each sequence of n images was formed and all such averaged images were uploaded into Adobe Photoshop v7.0. The average image with the highest TMRE fluorescence intensity was used to manually construct a grid on a pixel-by-pixel basis, serving henceforth as a template grid. To eliminate the

effects of nontranslational movement, myocytes with considerable nontranslational movement were identified and not included in the analysis. Mitochondria consisted of 34.38 ± 15.04 pixels (N=9 myocytes) and the translational movement that was encountered never exceeded two pixels at a time. In addition, signals of mitochondria with a very small number of pixels usually were both rare and noisy and hence could not be treated as oscillating mitochondria. Furthermore, numerical identifiers for each element of the mesh, i.e. for single mitochondria within the myocyte, were selected (Figure 2.1).

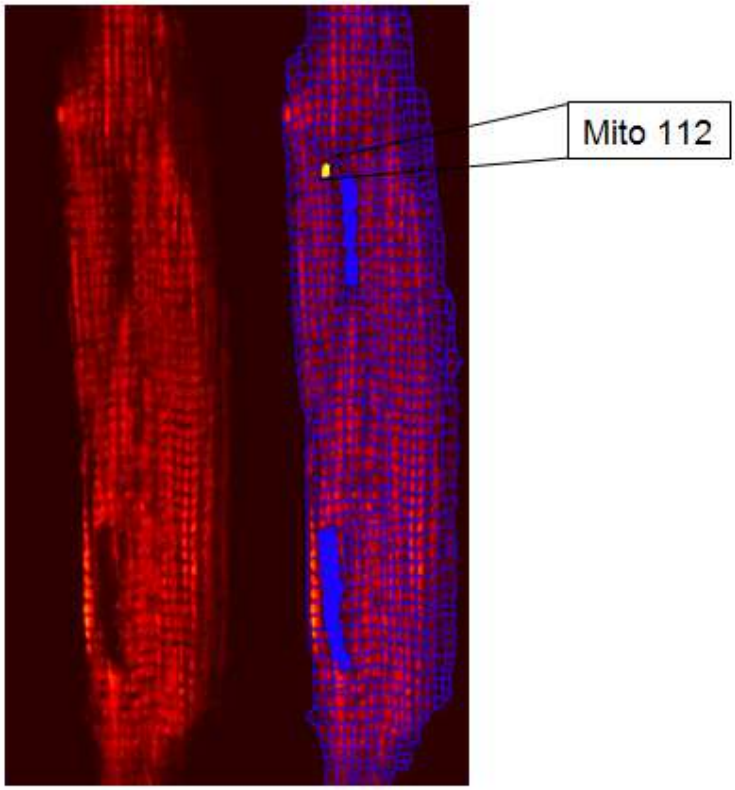

Figure 2.1 Identification of single mitochondria in cardiac myocytes. Single mitochondria of a myocyte are identified and labeled within a hand-drawn grid of an averaged stack of images in time.

2.2.2 *Extraction of individual mitochondrial membrane potentials*

Further processing in ImageJ (v.1.40g) was used to mark the overall shift in x- and y-direction of the myocyte of each averaged frame. The template grid was then shifted accordingly as a whole, thus providing an interval-independent mesh for each mitochondrion. Then, the TMRE intensity in each mesh was obtained by taking the average pixel TMRE intensity in that mesh.

2.2.3 Identification of mitochondrial nearest neighbors

If meshes of the template grid of any two mitochondria could be connected with a straight line that didn't cross more than one grid line, the corresponding mitochondria were considered to be nearest neighbors. For most mitochondria, this led to eight nearest neighbors, as in the case of a two-dimensional lattice.

2.3 Frequencies of oscillating mitochondria

2.3.1 *Wavelet analysis*

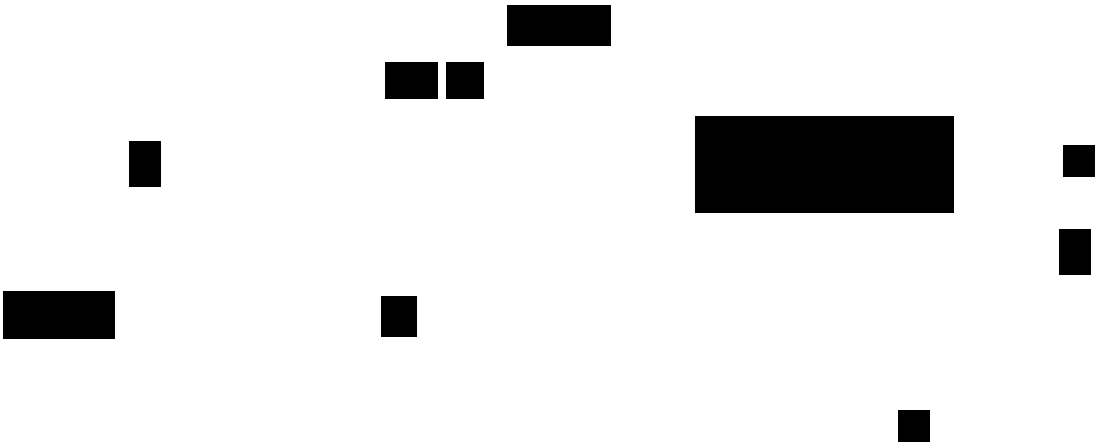

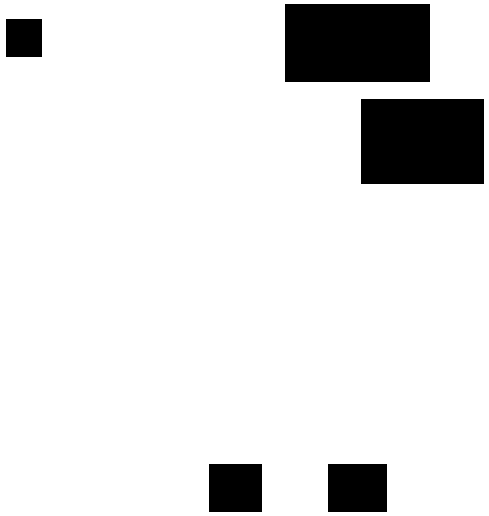

2.4 Selection and processing of individual mitochondrial TMRE signals in the whole heart

Whole heart samples were scanned for de- and repolarizing mitochondria: only myocytes showing at least one depolarization, i.e. a drop of more than 10% in TMRE fluorescence, of some of their mitochondria were taken into account.

Myocyte borders along sarcolemma and intercalated discs were manually applied on a pixel-by-pixel basis in Adobe Photoshop v7.0 (Figure 2.2). Grid templates were constructed for each selected myocyte and further spatio-temporal processing was done using wavelet analysis and major frequency cluster selection as in the case of the isolated myocyte.

2.5 Stochastic phase model

2.5.1 *Mitochondrial network architecture*

Identification of mitochondrial nearest neighbors was used as above to determine the mitochondrial network's structural morphology. To examine the network's connectivity properties, inter-mitochondrial coupling was only considered for local nearest-neighbor environments (Figure 2.3).

2.5.2 *Mitochondrial wavelet phase and wavelet frequency*

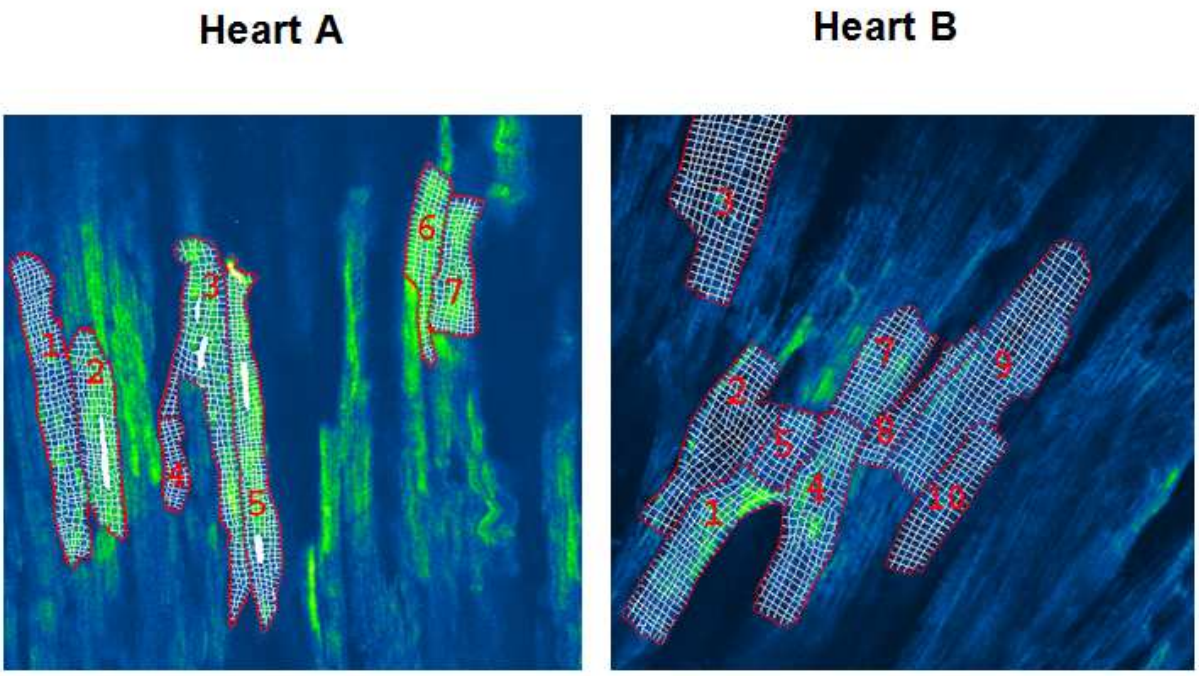

Figure 2.2 Patches of the intact heart of two guinea pigs. Cardiac cells were selected according to observed depolarization occurences. Myocyte borders along sarcolemma and intercalated discs were manually applied on a pixel-by-pixel basis (in red).

Wavelet phases were extracted from each individual mitochondrial TMRE signal as the wavelet transform coefficient's phase at maximal wavelet power as in the case of

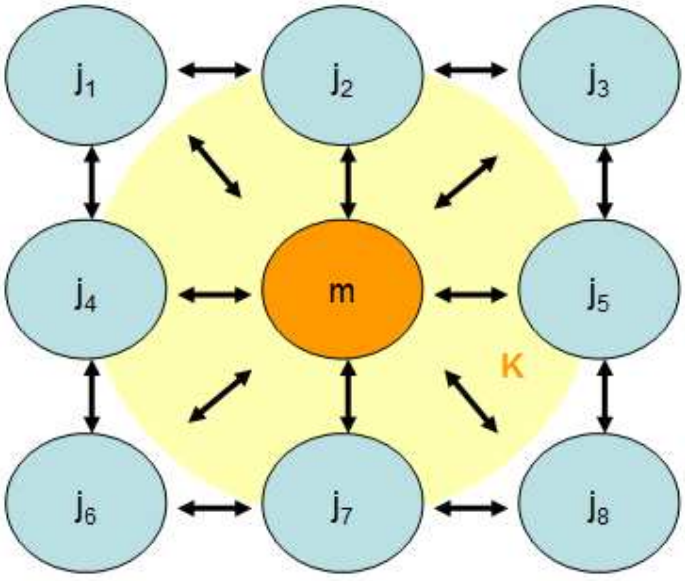

Figure 2.3 Scheme of the model's local coupling topology. Inter-mitochondrial coupling was only considered for local nearest-neighbors j_1, j_2,..., j_8 of mitochondrion m, thus providing an averaged coupling constant K for each mitochondrion m (symbolized by the beige colored cloud).

frequency. Wavelet frequencies are non-differentiable in time at points of frequency change, therefore, wavelet frequencies were taken as dynamical wavelet phase updates with the value of the actual wavelet frequency as starting point. The resulting updated wavelet frequency was median filtered to correct for frequency changes at the turning point of phase cycles.

2.5.3 *Ornstein-Uhlenbeck processes*

Within the stochastic coupling model of the mitochondrial network, mitochondrial intrinsic frequencies are modeled as frequencies that drift in time towards the respective measured mitochondrial frequency, i.e. the mitochondrial wavelet frequency. This accounts for dynamical changes in mitochondrial frequency and can be accomplished via Ornstein-Uhlenbeck processes that are described by the stochastic differential equation [79,92,93]

$$\frac{d\omega_m}{dt} = -\gamma(\omega_m - \mu_m) + \eta_m(t),$$

where μ_m represents the mean frequency towards which the intrinsic mitochondrial frequency is drifting to, η_m is a Gaussian white noise source with variance $\sigma_\eta^2 = 2\gamma\sigma_m^2$, γ represents the decay rate and σ_m^2 the amplitude of mitochondrial frequency fluctuations [78,79]. The mean frequency μ_m was chosen as the time-dependent wavelet frequency of the m-th mitochondrion, whereas the free constant γ was assumed to be identical for each mitochondrion in the network. The frequency fluctuation amplitude measure σ_m, for each mitochondrion, was taken as the standard variation of the measured mitochondrial wavelet frequency.

Discrete dynamical updates were performed to calculate the mitochondrial intrinsic frequencies [94]:

$$\omega_m(t+dt) = \omega_m(t)e^{-\gamma dt} + \mu_m(t)(1-e^{-\gamma dt}) + \sqrt{1-e^{-2\gamma dt}}\,\zeta \qquad (2.1)$$

where ζ is a random number drawn from a Gaussian distribution with zero mean and variance $\langle\zeta\rangle = \sigma_m^2$. Initially, $\omega_m(0)$ was taken from a Gaussian distribution with mean $\mu_m(dt)$ and variance σ_m^2.

2.5.4 *Local order parameter*

Local mitochondrial coupling was considered to be of local mean field type and

local mean field parameters $R_m(t)$ and $\psi_m(t)$ corresponding to mitochondrion m are defined as $R_m(t)e^{2i\pi\psi_m(t)} = \frac{1}{|L_m|}\sum_{j\in L_m} e^{2i\pi\varphi_j(t)}$, where L_m is the set of nearest neighbors of mitochondrion m (cf. [78,79]) and $|L_m|$ the number of its nearest neighbors. This corresponds to phase differential equations of the form

$$\frac{\partial\varphi_m(t)}{\partial t} = \omega_m(t) + K_m(t)R_m(t)\sin\left(2\pi(\psi_m(t)-\varphi_m(t))\right) \tag{2.2}$$

for each mitochondrion m.

2.5.5 *Update equations and Tikhonov regularization*

Within local mean field coupling, the left-hand side of equation (2.2) corresponds to the updated wavelet frequency ν_m^{WT} of mitochondrion m. This gives

$$\nu_m^{WT}(t) - \omega_m(t) \approx K_m(t)R_m(t)\sin\left(2\pi(\psi_m(t)-\varphi_m(t))\right).$$

Here, it is evident that K_m can become negative for some time points. However, in this model, it is assumed that the mitochondrial coupling constants are positive. This corresponds to the interpretation of an attractive coupling interaction between the oscillators, as was also originally assumed by Kuramoto [62,95]. Therefore, update equations for ω_m were subjected to the constraint

$$\frac{\nu_m^{WT}(t) - \omega_m(t)}{R_m(t)\sin\left(2\pi(\psi_m(t)-\varphi_m(t))\right)} > 0$$

for all timepoints.

In addition, solving for $K_m(t)$ proves difficult at points t_0 with

$$\lim_{t\to t_0} R_m(t)\sin\left(2\pi(\psi_m(t)-\varphi_m(t))\right) \to 0.$$

If one or more of such points existed for mitochondrion m, Tikhonov regularization was applied [96,97]. Setting

$$\mathrm{P}_m(t) = R_m(t)\sin\left(2\pi(\psi_m(t)-\varphi_m(t))\right),$$

this gives the explicit solution

$$\hat{K}_\mathrm{m} = (\mathrm{P}_m^2 + \lambda 1_T)^{-1}\mathrm{P}_m^T(\nu_\mathrm{m}^\mathrm{WT} - \omega_\mathrm{m})$$

with 1_T as the unity matrix of size T (T being the recording time) and Tikhonov parameter λ [97]. Optimization for λ was done using the Hanke-Reus algorithm [96] on

the interval $[(1/100)\cdot M, 100\cdot M]$ where $M = \sqrt{\| \mathrm{P}_m \|^2}/T$ is the time-averaged value of $\mathrm{P}_m(t)$. The Tikhonov parameter λ was put $\lambda = \frac{T}{100}\sqrt{\| \mathrm{P}_m \|^2}$ when the optimization did not converge. Each curve $K_m(t)$ was padded for $t < 0$ and $t > T$ with the mirror values of $K_m(t)$ for the respective vertical mirror axes at $t = 0$ and $t = T$ and the resulting curves were subsequently median filtered.

2.5.6 *Optimization of decay rate parameter* γ

Maximum likelihood estimation was applied to optimize the model parameter γ within the interval $[0,1]$. Basically, γ was taken along the interval in steps of 0.01 to calculate γ-dependent mitochondrial coupling constants $K_m(t,\gamma)$. All coupling constants $K_m(t,\gamma)$ were consequently averaged over Ornstein-Uhlenbeck frequencies with two different starting points $\omega_m(0)$ and two differently dynamically evolving ω_m.

In the next step, the $K_m(t,\gamma)$ were put in equation (2.2) together with the local mean field parameters R_m and ψ_m and random Ornstein-Uhlenbeck frequencies ω_m to forward model the mitochondrial phases $\varphi_m^{FM}(t,\gamma)$. The corresponding signal $\frac{1}{N}\sum_m \cos\left(\varphi_m^{FM}(t,\gamma)\right)$, N being the total number of mitochondria, was compared for each γ against the cosine of the phase of the overall TMRE signal of the myocyte by determining the least square error. γ-dependent error values were plotted versus γ and, if they were asymptotically approaching a fixed error value, exponentially fitted using an exponential function of the type $f(x) = a\cdot\exp(-bx) + c$ (Figure 2.4), where a, b and c are mathematical constants. Increasing in steps of 0.01 starting from 0, the optimal decay rate parameter for each cell was chosen as the first γ whose error value was within 1% range of the value of the asymptotic error value. If γ did not asymptotically approach a fixed error value but displayed instead a global minimum in the error values, the optimal γ was taken at this minimum.

2.5.7 *Coupling constants*

With optimal decay rate parameter γ_{opt} the coupling constants $K_m(t,\gamma_{opt})$ were

evaluated for 10 different starting points $\omega_m(0)$ and 100 differently dynamically evolving Ornstein-Uhlenbeck frequencies ω_m, respectively as above.

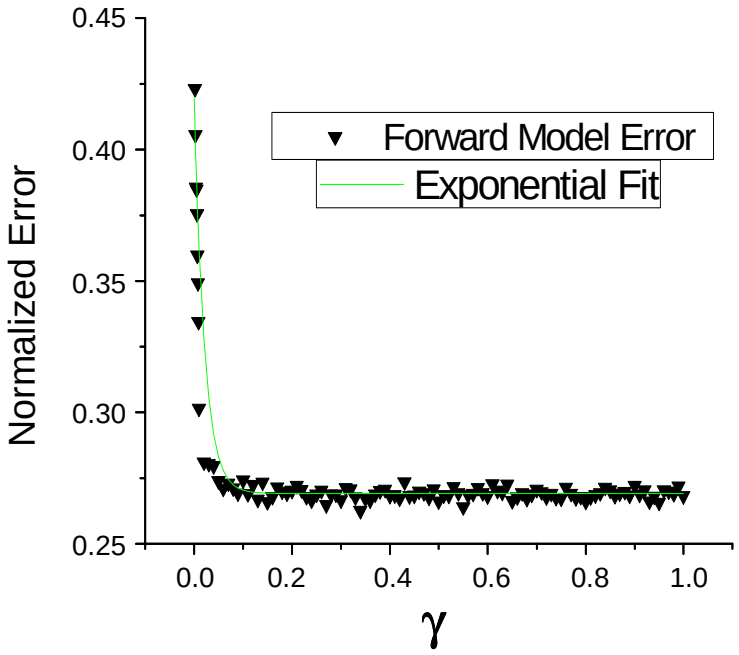

Figure 2.4 Normalized error of forward modeled γ-dependent stochastic phase model versus γ for a glucose-perfused cardiac myocyte. Exponential fit curve of type $f(x) = a \cdot \exp(-bx) + c$ in green. Increasing in steps of 0.01 starting from 0, the optimal decay rate parameter was chosen as the first value of γ whose error value was within 1% range of the value of the asymptotic error value (here, γ = 0.12).

2.6 Statistics

The wavelet analysis and fitting routines were obtained using Matlab v7.1.0.246 (R14). Further statistics were performed using OriginPro 8 SR0 v8.0724 (B724). Statistical significance ($p<0.05$) was obtained using the Mann-Whitney-test (in subsection 3.7) and the Kolmogorov-Smirnov test (in subsection 3.11.2, Figure 3.18).

III Results

3.1 Time-dependent frequency analysis of individual mitochondria using wavelet analysis

Figure 3.1

Figure 3.2

Figure 3.3 .

3.2 Algorithm for the selection of mitochondria belonging to a major cluster

To determine the frequency distribution of an oscillating mitochondrion and its relationship to neighboring mitochondria, a procedure was followed that is based on obtaining frequency histograms for all mitochondria. For each frame i , the instantaneous individual mitochondrial frequencies were obtained with the wavelet method as described above and by plotting their distribution the maximum peak ($P_{\mathbf{max}}^{(i)}$) value as shown in Figure 3.4 could be determined. Then, all relevant histogram peaks were identified as those frequencies whose histogram amplitude is above 10% of $P_{\mathbf{max}}^{(i)}$ (Figure 3.4).

Additional adjacent peaks above 10% of $P_{\mathbf{max}}^{(i)}$ were identified and considered as part of the same or different cluster, as follows. For each such peak, the mean TMRE

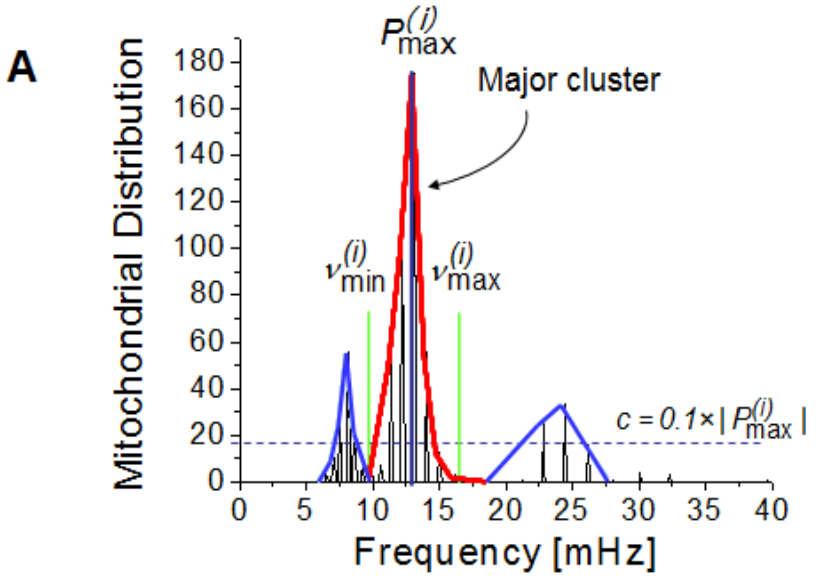

Figure 3.4 Frequency histogram for a specific frame obtained from wavelet analysis. There are three apparent major clusters. The amplitude distribution cut-off ($c = 0.1 \cdot \left|P^{(i)}_{\max}\right|$) is marked with a horizontal dashed line, the minimum and the relevant cluster peak $P^{(i)}_{\mathbf{max}}$ (in red) extends to frequencies defined by $\nu^{(i)}_{\min}$ and $\nu^{(i)}_{\max}$ (green lines). Since the correlation of the other two clusters peaks (in blue) with the major cluster peak is lower than 95%, the major cluster peak does not include these smaller clusters.

signal as well as the lowest and highest frequencies of the peak were determined by interpolating the non-zero frequency amplitudes within the peak.

Then, the correlation coefficient of the mean TMRE signal of mitochondria corresponding to the $P^{(i)}_{\mathbf{max}}$ peak was obtained, with the mean TMRE signal of mitochondria belonging to each of the adjacent identified peaks over a running window (T_w). To capture frequencies in the range of the largest period of oscillation in the mean TMRE fluorescence plot, the size of the running window was chosen such that it is equal to 1.1 times the duration of the period of that oscillation.

If the mean TMRE signal of an adjacent peak had a correlation coefficient that was greater than 95% with the mean TMRE signal of $P^{(i)}_{\mathbf{max}}$ peak, then the adjacent peak was incorporated into the $P^{(i)}_{\mathbf{max}}$ peak. The procedure was repeated for both higher and lower frequencies with respect to $P^{(i)}_{\mathbf{max}}$, until the correlation coefficient dropped below 95%.

At this stage, a frame-dependent distribution of frequencies was derived that is likely to belong to a major cluster of oscillating mitochondria. Additionally, the mean

TMRE signal of all mitochondria in the refined distribution of mitochondria around $P_{\mathbf{max}}^{(i)}$ was cross-correlated with the TMRE signal of each mitochondrion that did not belong to the major cluster. If the correlation coefficient of a single mitochondrion was above 95%, that mitochondrion was further incorporated into the major cluster, thus determining all oscillating mitochondria that belonged to the major cluster in a given frame. The latter approach was necessitated by the need to account for the case in which the cut-off 10% of $P_{\mathbf{max}}^{(i)}$ was too strict, and therefore could potentially reject mitochondria in which the TMRE signal was highly correlated with that of the major cluster.

3.3 Cluster-frequency and cluster-size relationship

To examine the relation between cluster-frequency and cluster-size the mean radius of the cluster was defined by taking the distance of the pixel of the geometrical center of the cluster to each single mitochondrion's geometrical center and dividing it by the number of cluster mitochondria for each frame.

Then, the mean radius of the cluster mitochondria was plotted against the mean frequency of the cluster (Figure 3.5), the relative area of the cluster mitochondria (quotient of total cluster pixel-count and myocyte pixel-count) against the mean frequency of the cluster (Figure 3.5C) and the relative number of cluster mitochondria (quotient of the number of cluster mitochondria versus the total number of mitochondria) against the mean frequency of the cluster (Figure 3.5D), for each frame. As can be clearly seen, there is an inverse relationship between mitochondrial cluster size, area and number versus the mean frequency of the cluster which suggests that large clusters have a longer oscillation period than small ones.

Subsequently, the frequency distribution of the mitochondria belonging to the major clusters was examined. For each cardiomyocyte, a frequency histogram of all mitochondria belonging to a major cluster was obtained, across all frames (Figure 3.5E). Mitochondrial frequencies were counted in bins of width 0.1 mHz in the range [0 - 50] mHz.

Specifically, to allow comparisons between myocytes, the counts of each frame were divided by the number of the mitochondria belonging to a major cluster in that frame, and the amplitude at each frequency in the frequency histogram was again divided by the total number of frames. Then, a final histogram was created and

fitted to a Gaussian function. The frequency bandwidth within two standard deviations of the Gaussian fit was determined to be: 8.73 - 22.3 mHz. Using Figure 3.5B, this indicates that the mean radius of the oscillating cluster of mitochondria is between 27 - 30 μm. The relatively high standard error in this region of the plot results from gaps in the major cluster of mitochondria. In fact, such a non-contiguous mitochondrial cluster, with mitochondria that oscillate close to the same frequency (a "frequency cluster"), shows a similar topology to that described in spanning clusters [21,36]. Specifically, we have observed that in some myocytes, the major frequency cluster shows many non-cluster areas of mitochondria at the onset of oscillations, while during the course of recording more and more of these gaps between frequency cluster mitochondria are filled, yielding a more contiguous morphological cluster. Thus, from Figure 3.5A, the rate of change of mean radius with respect to the frequency was calculated to be: -0.0973 ± 0.13 μm/mHz.

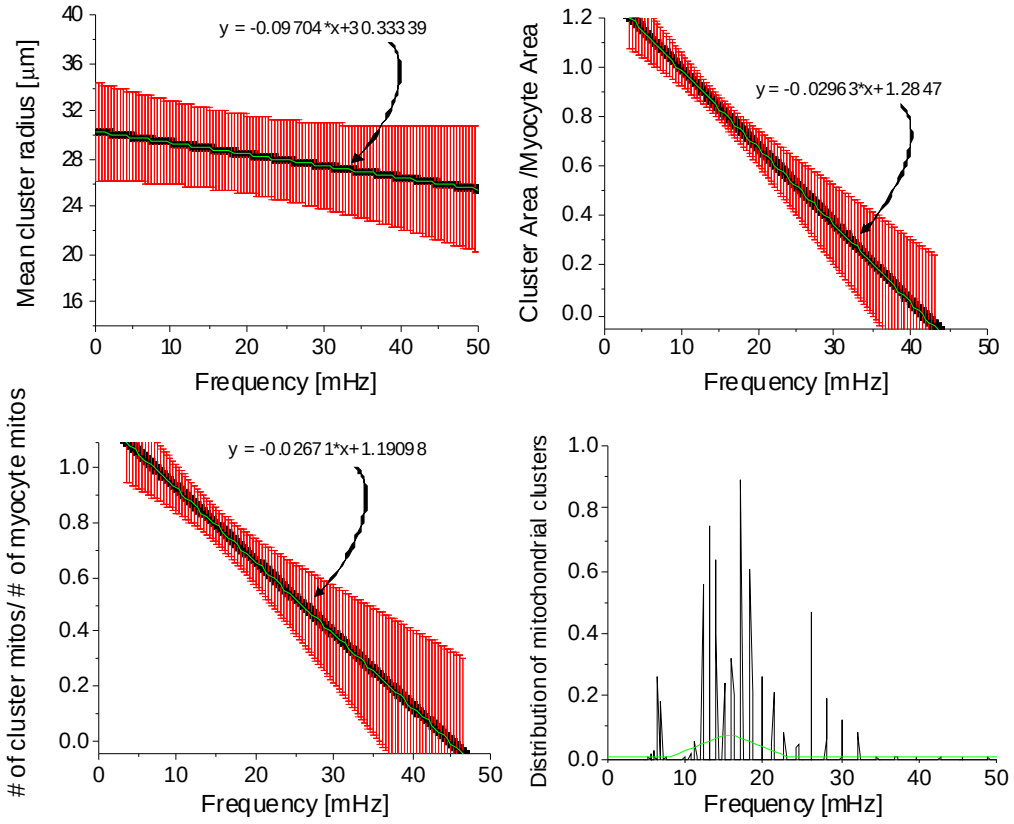

Figure 3.5 Mitochondrial frequency distribution in clusters for different myocytes (N=9). (A) Mean cluster radius as a function of frequency. (B) Cluster area normalized by the full myocyte area as a function of frequency. (C) Cluster mitochondria count normalized by the total number of mitochondria for the major cluster as a function of frequency. Standard error bars are shaded in red and the mean curve in black. (D) Distribution of mitochondrial frequencies for all cluster mitochondria across all myocytes.

However, it was observed that the % area of the cluster, defined as the quotient of the area of cluster mitochondria and whole myocyte area (Figure 3.5C), or the % number of cluster mitochondria, defined as number of cluster mitochondria divided by the number of mitochondria in the cardiomyocyte (Figure 3.5D), are measures with less uncertainty of the cluster size. The % area of the cluster changes by -2.96 ± 1.11 % / mHz and the % number of cluster mitochondria by -2.67 ± 1.12 % / mHz.

3.4 Cluster oscillation coherence

To analyze the temporal properties of the cluster mitochondria, the temporal coherence properties of cluster mitochondria were investigated by estimating the average coherence of the TMRE signal of each cluster mitochondrion with its nearest neighbors. Coherence takes values between 0 and 1 at each frequency, indicating whether two signals oscillate in synchrony (“1”) at each frequency or not (“0”).

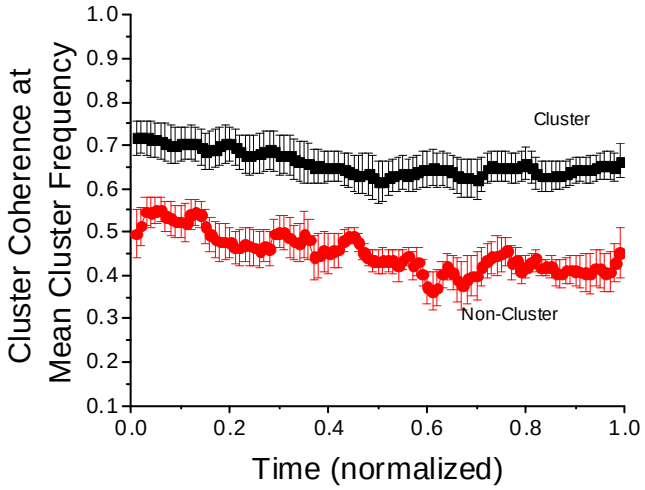

Figure 3.6 Coherence of mitochondria belonging to the major oscillating cluster, estimated at the mean cluster frequency (N=9). For statistical comparison among myocytes with unequal recording durations, the duration of the oscillations of each recording was normalized.

The coherence of each cluster mitochondrion was estimated in Matlab with a running window of size T_w and a fixed FFT length of $2^{11}dt$. Frequency ranges for each myocyte were taken from zero to 100 mHz and divided into $(2^{11}/2)+1$ segments, therefore each segment represented approximately 0.1 mHz. As windowing function for Matlab’s mscohere function (over each running window) a Hamming window with length

$T_w / 8$ was applied.

The coherence was then obtained for each cluster mitochondrion in the specific running window by taking the average coherence at each frequency over all nearest neighbors that belonged to the cluster. Subsequently, another averaging of the coherence was performed over all cluster mitochondria. This process was continued by shifting the running window by one frame at a time until the last frame of the current running window was equal to the last frame of the recorded signal. Finally, for each running window the value of the mean coherence at the mean frequency of all mitochondria belonging to the cluster was estimated, thus obtaining the coherence as a function of time. To further compare myocytes with unequal duration of recordings, each cardiomyocyte's duration of oscillations was set to 1.

One observes that the coherence of the cluster mitochondria does not change significantly during the recording, indicating a high temporal stability of the coherence of the oscillating cluster mitochondria (Figure 3.6, in black). Averaging over time yields a coherence of 0.66 ± 0.04. In comparison, the coherence for non-cluster mitochondria (Figure 3.6, in red) was determined to be 0.44 ± 0.04, which demonstrates, in a quantitative manner, that non-oscillating mitochondria are less correlated with each other than those within the cluster. Nevertheless, it should be noted that despite the profound difference in coherence between cluster and non-cluster mitochondria, the non-cluster mitochondria still exhibited quite a high degree of coherence. This may be attributed to the fact that non-cluster mitochondria might oscillate too; however, at a different inherent frequency compared to those within the cluster.

3.5 Mitochondrial oscillation amplitude versus cluster size and cluster frequency

In the next step, the relationship between oscillation amplitude and cluster size was examined. The mean TMRE signal of the mitochondrial cluster was determined, each peak manually identified. The time- (Δ_t) and the peak-trough amplitude difference (Δ_a) of the TMRE intensity were determined (Figure 3.7A). The mean frequency and area (in pixels) of the cluster mitochondria for all frames within Δ_t were then determined and averaged over Δ_t. For each myocyte, and for each Δ_t, the mean cluster area normalized to the area of the full myocyte was plotted against the corresponding TMRE amplitude normalized to the maximum amplitude (Figure 3.7B, slope: -0.29 ± 0.1). The quotient of cluster amplitude over the cluster area was determined as a function of the

mean cluster frequency in the same time-range (Δ_t), suggesting that there is a negative correlation between cluster size and cluster amplitude (Figure 3.7B). However, it should be noted that this result does not suggest that the extent of depolarization is smaller when the cluster size increases, but rather that it reflects more prolonged and incomplete repolarization of the network between oscillations (see Figure 3.7A). The rate of change of the cluster amplitude versus frequency is larger than that of the cluster area (Figure 3.7C, slope: 0.14E-2 ± 0.06E-2 /mHz).

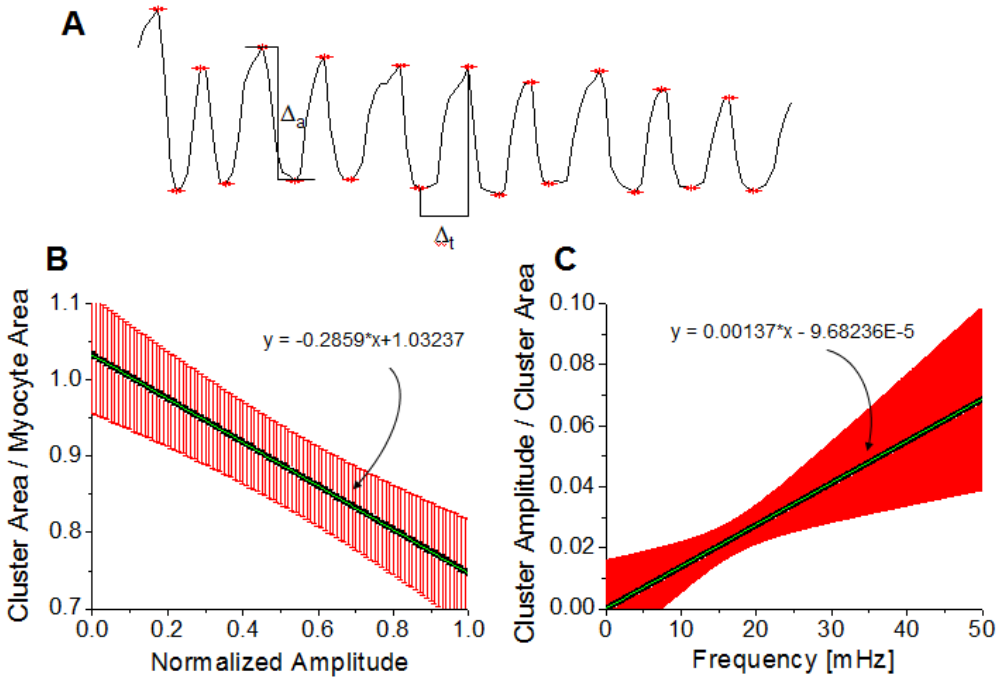

Figure 3.7 (A) Method for selecting the amplitude of the oscillation. After selecting peaks of the mean TMRE signal of a major cluster of mitochondria, the mean cluster area and frequency between consecutive peaks were determined as well as the amplitude as the difference in their TMRE intensity. (B) Oscillation amplitude values are normalized by the maximum amplitude value and are plotted against the normalized cluster area (N=8). (C) Mitochondrial amplitudes normalized by the cluster area follow a linear pattern when plotted against the mean cluster frequencies (N=6).

3.6 Isochronal mapping

To gain a better understanding of the dynamics of mitochondrial $\Delta\Psi_m$ at the onset (spatio-temporal) of synchronized depolarizations for a myocyte subjected to a localized laser flash (indicated by a red square in Figure 3.8), an isochronal map of mitochondrial earliest depolarization at the time of the maximum first derivative of the

TMRE signal (Figure 3.8) was created.

Only mitochondria with a clear and distinctive depolarization slope were taken into account, while missing mitochondria were 2D-interpolated using Matlab. The isochronal map was created by displaying the activation time of each mitochondrion with respect to the earliest activation time across all mitochondria.

As can be seen in Figure 3.8, the first mitochondria depolarized at the bottom left of the myocyte and the depolarization spread towards both ends of the cell along the longitudinal axis. It is remarkable that in this myocyte (from a canine heart), it is not the flashed mitochondria (signified with a red square) that trigger the first depolarizations, but instead an initial nucleus of synchronized mitochondria slightly separated from the

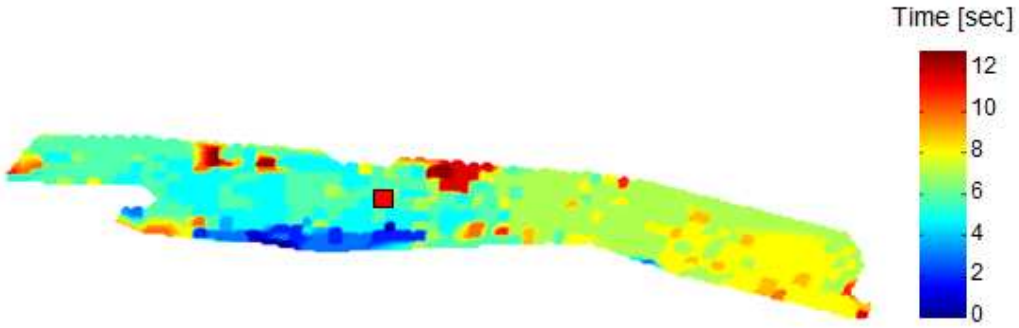

Figure 3.8 Isochronal Map of a canine cardiac myocyte at the onset of flash-triggered oscillations. The red square signifies the area of the flash. Isochrones are taken as the difference of maximum slope derivative time-points over all mitochondria. About 25 seconds after the flash an initial critical mass of mitochondria in the left bottom area of the myocyte triggers mitochondrial depolarizations by exciting a critical number of mitochondria. The excitation penetrates the whole myocyte within approximately 10-12 seconds, thus leading to a conduction velocity of about 32 μm/sec.

flashed region was created. This observation is in agreement with prior observations that suggest that myocyte-wide mitochondrial oscillations originate from a nucleus of mitochondria [21,22,36], that does not necessarily have to be fixed in only one place.

Assuming that the depolarization spreads uniformly from the geometrical center of the initiating nucleus of mitochondria to the farthest ends of the myocyte, which in this example took ~10 s to complete, a longitudinal conduction velocity of ~32 μm/sec was obtained, which is close to that measured in flash-triggered guinea pig myocytes (22 μm/sec) [36].

3.7 Longitudinal versus transverse correlation of mitochondrial membrane potential

To quantitatively examine $\Delta\Psi_m$ wave propagation differences in the longitudinal versus transverse directions, two axes were selected: a longitudinal axis parallel to the cardiac myocyte myofilaments and a transverse axis perpendicular to the myofilaments (Figure 3.9). For a single cluster mitochondrion {*i*} at each frame, the neighboring mitochondria belonging to the major cluster along each axis were determined. TMRE signals of the transverse or longitudinal neighbors of a

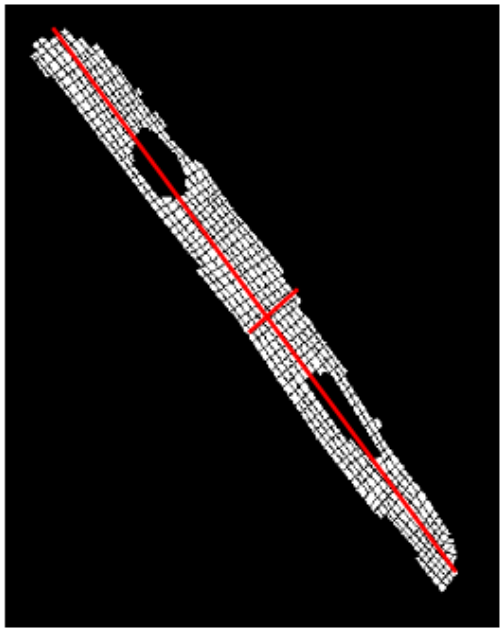

Figure 3.9 Difference in signal correlation of longitudinal and transversal cluster neighbors. The longitudinal axis is selected against the striae of the myocyte.

mitochondrion {*i*} of the cluster were cross-correlated with that mitochondrion over a running window of length T_w, and the average correlation coefficient (CC) along each axis yielded a time- and mitochondria-specific longitudinal and transversal CC.

In Table 3.1, we see that the values of the longitudinal and transverse correlations are significantly different from each other. Since the longitudinal correlation is stronger than the transversal one, this finding suggests that the longitudinal axis is the preferred axis of depolarization propagation. This is in keeping with the spatial organization of the mitochondrial network, where polarized mitochondria are usually

distributed in rows along the longitudinal axis and very rarely in single rows along the transverse axis (with some deviation from this generalization for mitochondria located between the nuclei of the cell). This could be related to diffusional restrictions imposed by the spatial arrangement of the myofilaments which separate the mitochondria in the transverse direction [99].

	Mean value	**StdE(±)**
longitudinal CC	0.8072	3.3494E-4
transversal CC	0.7071	4.353E-4
longitudinal CC / transversal CC	1.2657	0.0804

Table 3.1 Longitudinal and transversal correlation of cluster mitochondria. Correlation coefficients of direct cluster neighbors of cluster mitochondria are averaged along each axis and evaluated for all images in different myocytes (N=7).

3.8 Cluster frequency and cluster size relationship in isolated cardiac myocytes for perfusion with different substrates

Preceding wavelet-based analyses of individual mitochondrial inner membrane potential, TMRE fluorescence oscillations in cardiac myocytes in the pathophysiological state provided a dynamic frequency for each oscillating mitochondrion. In addition, it could be determined if a mitochondrion belonged to a cluster of mitochondria with similar frequencies, a frequency cluster that should not be thought of as a morphologically connected cluster, for each sampling point of the recording. While only considering those oscillating mitochondria that belong to the major frequency cluster, the overall cluster size was found to be inversely correlated with the cluster's mean frequency. This indicates decelerated cluster synchronization to a common oscillatory mode for larger clusters due to prolonged diffusion-mediated processes within the coupling medium [100,101]. However, the underlying experiments were performed on isolated cardiac myocytes perfused with a glucose solution. But it remained unclear if the same spatio-temporal mitochondrial network properties apply to patches of intact heart tissue. Likewise, there were no previous studies about mitochondrial frequency cluster dynamics in cardiac myocytes that are perfused with metabolic agents other than glucose.

Major cluster mitochondria were determined for each myocyte of each set of cells treated with pyruvate, lactate and β-hydroxy-butyrate, respectively. Subsequently, measures for cluster-size were compared with the mean frequency of the cluster mitochondria. For this purpose, the mean cluster radius was plotted against the mean frequency of the cluster (Figure 3.10).

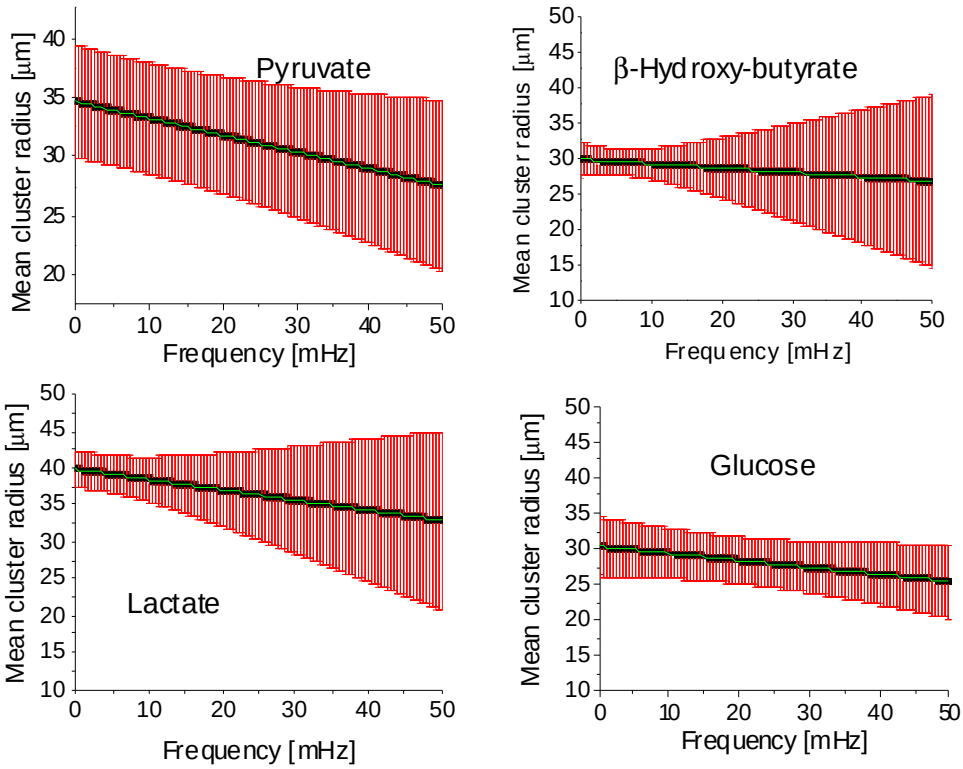

Figure 3.10 Mean cluster radius as a function of frequency for isolated cardiac myocytes perfused with pyruvate(N=10), β-hydroxy-butyrate (N=14), lactate (N=7) and glucose (N=9) respectively.

Similarly, the relative area of cluster mitochondria and the relative number of cluster mitochondria were each plotted against the mean frequency of the cluster (Figures 3.12-13). The inverse relationship between mean mitochondrial cluster radius, relative cluster area and number is obvious and is similar to the results in glucose-treated cardiac myocytes. This suggests that, throughout all sets of cells that are treated with respective substrates, large clusters have a longer oscillation period than small ones.

Frequency distributions of mitochondria belonging to the major cluster were

constructed with frequency histograms across all frames (Figure 3.11) for each cardiac myocyte in each substrate group as detailed above. This has already been demonstrated for glucose-treated myocytes to give a frequency bandwidth of 8.7 - 22.3 mHz. In comparison, pyruvate-treated myocytes show a more dispersed frequency distribution that ranges from 3.7 - 54.8 mHz, whereas myocytes from the lactate group are more narrowly distributed with frequencies in the range 3.9 - 15.0 mHz. Myocytes

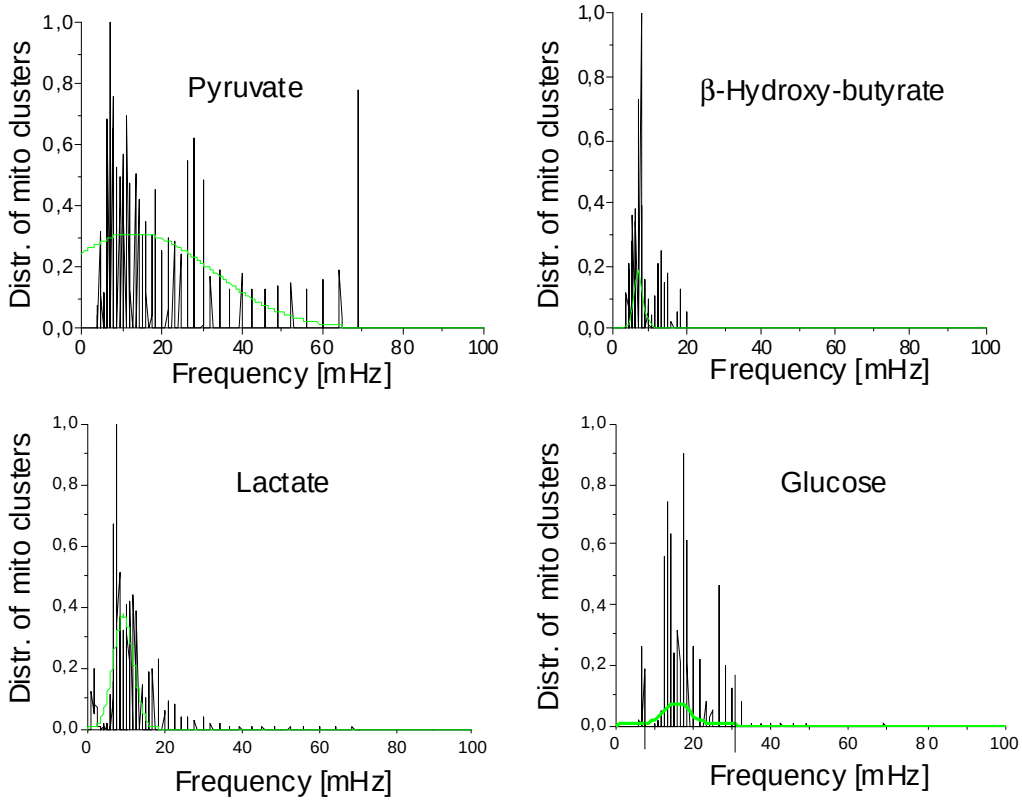

Figure 3.11 Distribution of mitochondrial frequencies for all cluster mitochondria across all cardiac myocytes perfused with pyruvate(N=10; A), β-hydroxy-butyrate (N=14; B), lactate (N=7; C) and glucose (N=9; D) respectively.

that were treated with β-hydroxy-butyrate displayed mostly major cluster oscillations in the low frequency range of 4.0 - 10.1 mHz. With Figures 3.10, this indicates that the mean radius of the oscillating clusters of mitochondria for glucose-, pyruvate-, lactate- and β-hydroxy-butyrate-treated myocytes is ~27 - 30 μm, ~27 - 35 μm, ~37 - 40 μm and ~29 - 30 μm, respectively. High standard errors in Figures 3A are, again, due to topological non-contingencies of the mitochondrial major clusters, indicating a distribution of major cluster mitochondria similar to spanning clusters (cf. [21,36]).

It has been observed that with the onset of synchronized depolarization, in some myocytes, major frequency cluster mitochondria appear dispersed throughout the cell but grow more and more to be topologically contiguous during the course of recording. However, non-contiguous cluster mitochondria with a high degree of differently oscillating mitochondrial clusters have especially been observed for pyruvate-treated

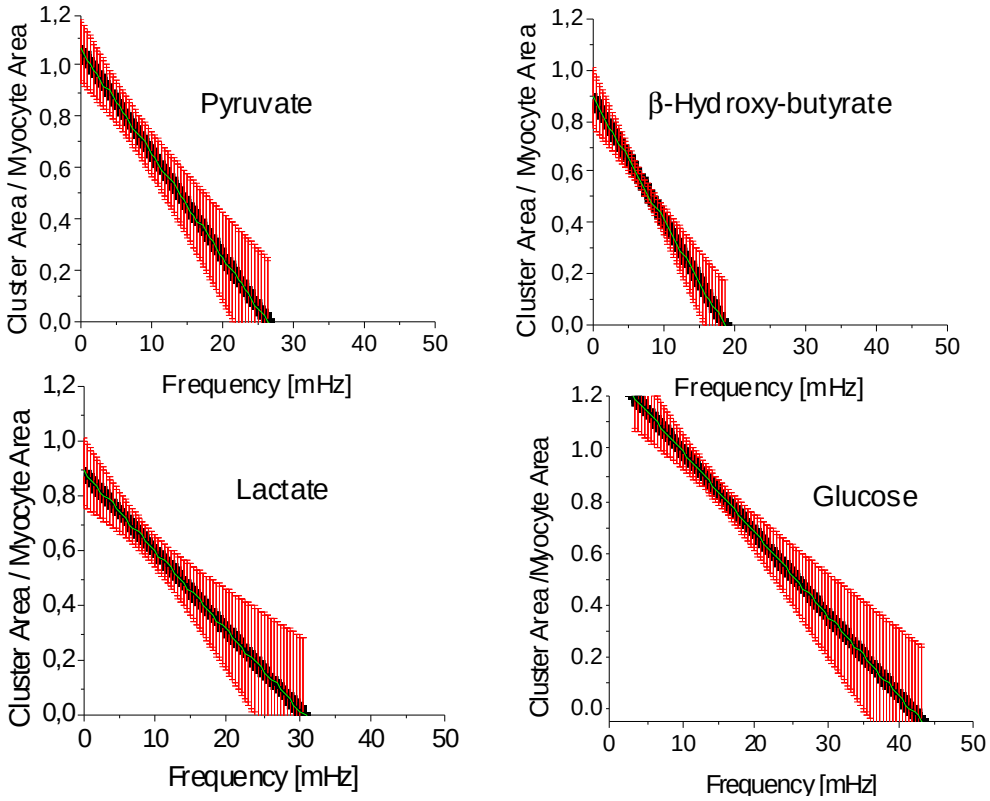

Figure 3.12 Cluster area normalized by the full myocyte area as a funtion of frequency for isolated cardiac myocytes perfused with pyruvate(N=10; A), β-hydroxy-butyrate (N=14; B), lactate (N=7; C) and glucose (N=9; D) respectively.

cells as well as in the case of glucose-bathed tissue slices of the intact heart with no significant growth in contiguity. The rate of change of mean radius with respect to the frequency for myocytes from the glucose-, pyruvate-, lactate- and β-hydroxy-butyrate-group have been calculated to be: -0.0973 ± 0.129 μm/mHz, -0.141 ± 0.017 μm/mHz, -0.139 ± 0.018 μm/mHz and -0.060 ± 0.016 μm/mHz, respectively.

Better measures of cluster size can be given by % area of the cluster (Figure 3.12) or % number of cluster mitochondria (Figure 3.13). The rate of change of % area

versus frequency for glucose-, pyruvate-, lactate- and β-hydroxy-butyrate-treated cardiac myocytes was given as -2.96 ± 1.11 % / mHz, -4.01 ± 0.07 % / mHz , -2.90 ± 0.07 % / mHz and -4.86 ± 0.07 % / mHz, respectively and, likewise, the % number of cluster mitochondria was determined to be -2.67 ± 1.12 % / mHz, -4.01 ± 0.07 % / mHz ,

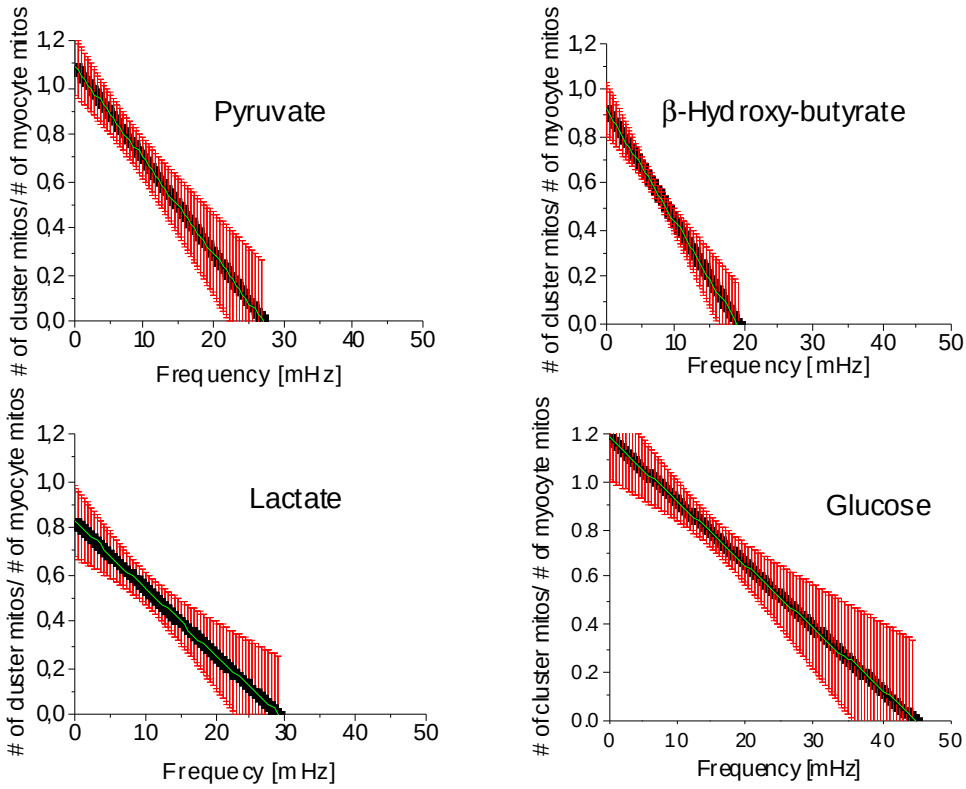

Figure 3.13 Cluster mitochondria count normalized by the total number of mitochondria for the major cluster as a function of frequency for isolated cardiac myocytes perfused with pyruvate(N=10; A), β-hydroxy-butyrate (N=14; B), lactate (N=7; C) and glucose (N=9; D) respectively.

-2.83 ± 0.07 % / mHz and -4.79 ± 0.07 % / mHz. It appears that cardiac myocytes from the β-hydroxy-butyrate group show the strongest change of % area versus frequency, i.e. about 64% more than glucose-treated cells. Pyruvate-treated myocytes show a rate of change of % area versus frequency that is approximately 35% higher than myocytes from the glucose group. Cardiac myocytes from either lactate or glucose group exhibit similar rates of change of % area versus frequency.

In addition, cells from the β-hydroxy-butyrate group show % area versus

frequency changes at moderately low frequencies below 20 mHz, whereas the other substrate groups exhibit % area changes at slightly higher frequencies, especially in glucose-treated cardiomyocytes.

3.9 Cluster oscillation coherence for different substrates

There is no significant change in the coherence of the cluster mitochondria during the recording in any of the substrate groups, thus indicating high temporal stability of the respective oscillating cluster mitochondria (Figure 3.14).

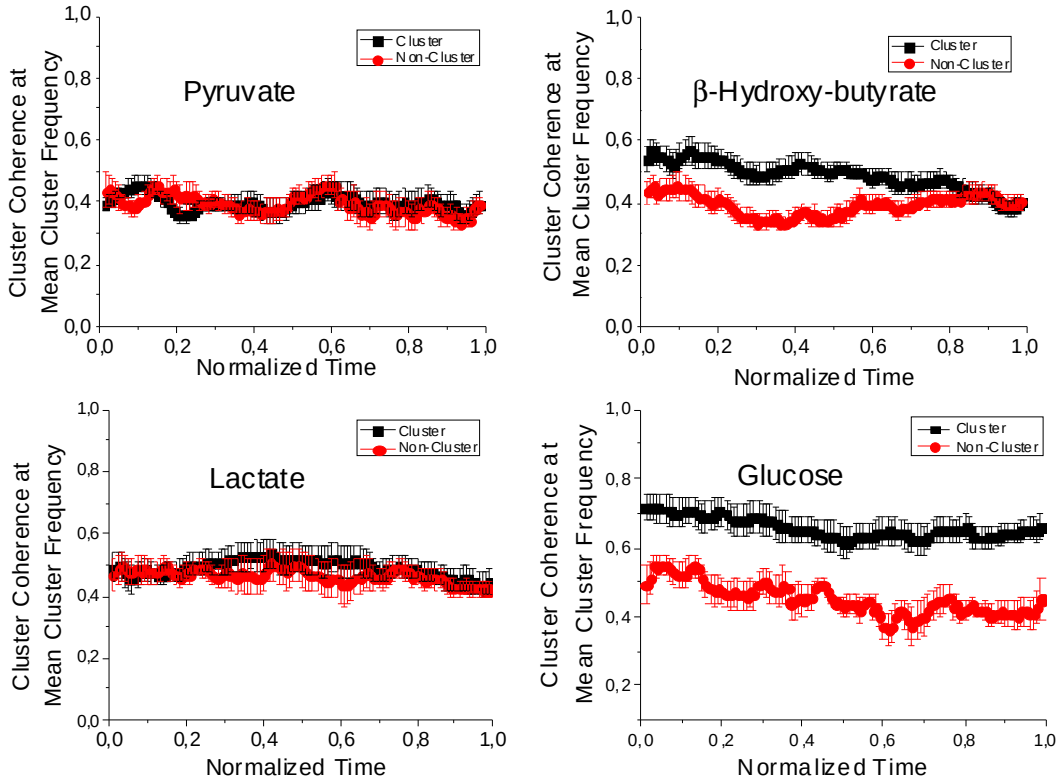

Figure 3.14 Coherence of mitochondria belonging to the major oscillating cluster, estimated at the mean cluster frequency for isolated cardiac myocytes perfused with pyruvate(N=10; A), β-hydroxy-butyrate (N=14; B), lactate (N=7; C) and glucose (N=9; D) respectively.

However, coherences of cluster mitochondria averaged over time seem to be highest 0.66 ± 0.04 in glucose-treated cardiac myocytes, whereas coherences in the pyruvate-, lactate- and β-hydroxy-butyrate substrate groups are 0.40 ± 0.03, 0.49 ± 0.04 and 0.49 ± 0.03, respectively. Coherences of mitochondria that do not belong to the

major cluster are estimated to be 0.44 ± 0.04, 0.39 ± 0.04, 0.46 ± 0.04 and 0.39 ± 0.03 for glucose-, pyruvate-, lactate- and β-hydroxy-butyrate-treated cardiac myocytes, respectively. Thus, non-cluster mitochondria coherence properties seem to be similar for perfusion with different substrates, exhibiting a relatively high degree of coherence. As suggested above, this may be due to stable oscillations of non-cluster mitochondria at frequencies that are different to the frequencies at which major cluster mitochondria oscillate. The difference already investigated in coherence between cluster and non-cluster mitochondria for glucose-treated myocytes remains valid for all substrates, although it is much less pronounced for lactate and pyruvate. A decreased level of synchrony during de- and repolarizations has been specifically observed in the case of pyruvate-treated cardiomyocytes, thus giving a smaller and more topologically dispersed ensemble of major cluster mitochondria. The alignment of temporal properties of a cluster mitochondrion with its neighboring mitochondria might therefore be less prominent, thus providing a lower coherence.

3.10 Cluster frequency and cluster size relationship in the intact heart

As in the case of isolated cardiac myocytes, major cluster mitochondria were found for each cardiac myocyte with signs of depolarization during TMRE recording in glucose-treated slices of the intact heart close to the left anterior descending coronary artery.

The rate of change of mean cluster radius with respect to the frequency for glucose-treated myocytes in two patches of the whole heart has been calculated to be: -0.14 ± 0.01 μm/mHz (heart A, Figure 3.15A.1) and 0.03 ± 0.01 μm/mHz (heart B, Figure 3.15B.1). Summary statistics of mitochondrial frequency distributions of major cluster mitochondria for all cardiac myocytes of the respective slice of the intact heart yield frequency ranges of 10.30 - 58.1 mHz (heart A) and 10.3 - 82.2 mHz (heart B). Evidently, the frequency range of mitochondrial frequencies in cardiac myocytes of the intact heart is significantly broader than that in isolated myocytes, i.e. mitochondria generally oscillate at higher frequencies. According to Figures 3.15A.1 and 3.15B.1 the mean cluster radius is ~11 - 17 μm for patch A and ~ 10 - 12 μm for heart B.

The rate of change of % area versus frequency for cardiac myocytes of two different slices of the intact heart was determined to be -2.44 ± 0.10 % / mHz (heart A) and -2.40 ± 0.13 % / mHz (heart B). Likewise, the % number of cluster mitochondria

versus frequency showed a rate of change of -2.37 ± 0.10 % / mHz and -2.27 ± 0.12 % / mHz, respectively. Therefore, for recordings with glucose-perfusion, the respective rate of change of % area and number versus frequency in whole heart cardiac myocytes is about 18-19% and 11-15% smaller than in isolated cardiac myocytes. Also, the results point out that clusters at whole cell level in slices of the intact heart have higher frequencies than those in isolated cardiac myocytes.

Again, for two examined tissue slices, the inverse relationship between relative cluster area and number, as observed in isolated cardiac myocytes, was confirmed. Therefore, this indicates that large clusters have a longer oscillation period than small ones not only in the case of isolated myocytes, but also for an intact ensemble of communicating cardiac myocytes. However, an inverse relationship between mean cluster radius and frequency could only be verified for one of the slices, hence it appears that formations of non-contiguous topological major clusters in the intact heart are much more likely than in isolated myocytes. Also, the mean cluster radius is found to be in µm-ranges about half the size as that of isolated glucose-treated cardiac

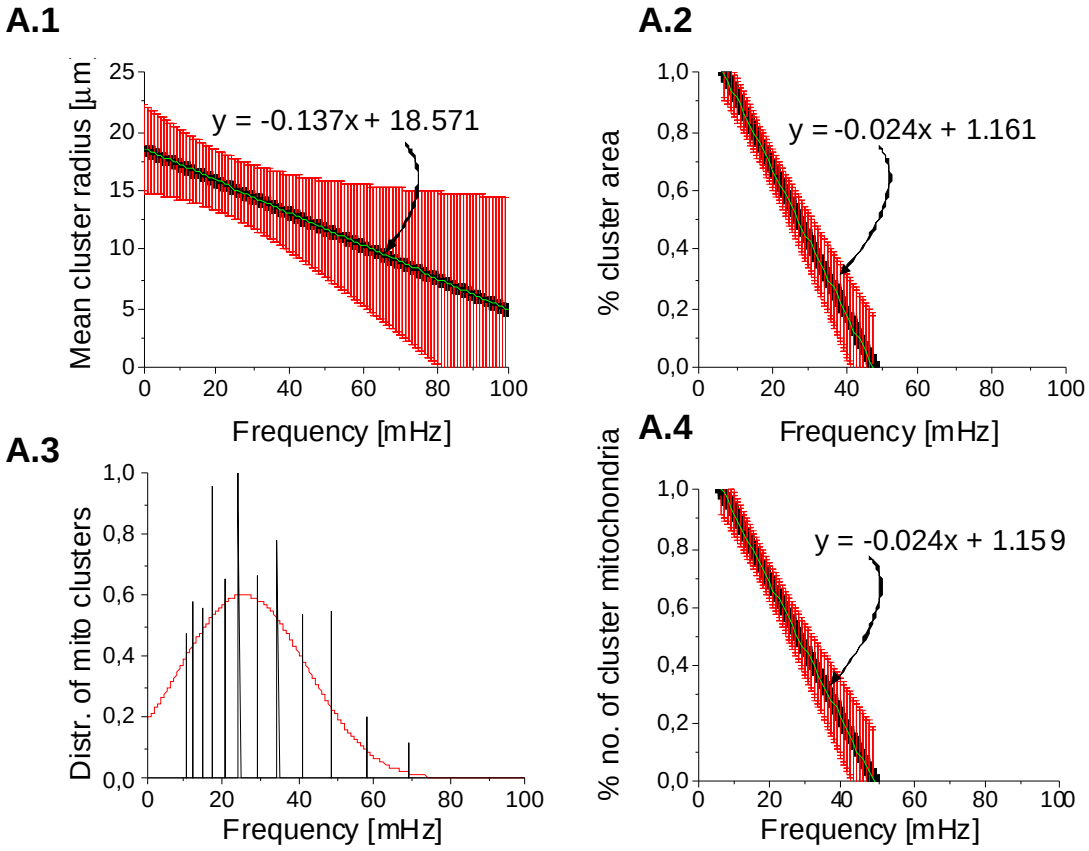

Figure 3.15 (continues on next page)

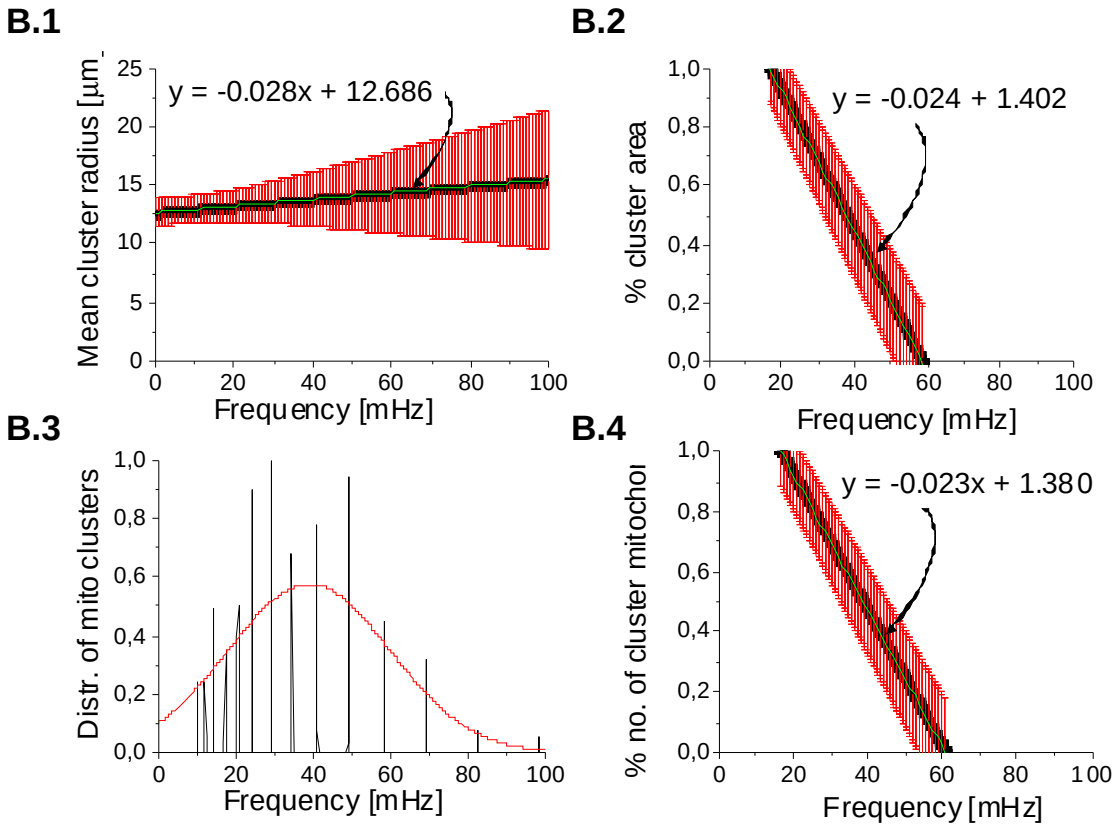

Figure 3.15 Mitochondrial cluster properties for patches of tissue in the intact heart for two different guinea pig hearts A (with 7 considered cardiac myocytes) and B (with 9 considered cardiac myocytes). (A.1-B.1) Mean cluster radius as a function of frequency. (A.2-B.2) Cluster area normalized by the full myocyte area as a funtion of frequency. (A.3-B.3) Cluster mitochondria count normalized by the total number of mitochondria for the major cluster as a function of frequency. Standard error bars are shaded in red and the mean curve in black. (A.4-B.4) Distribution of mitochondrial frequencies for all cluster mitochondria across all myocytes.

myocytes. Taken together, this suggests that major clusters in myocytes of the intact heart are more dispersed and generally smaller than in isolated myocytes, indicating an influence of inter-cellular communication on ROS formation and signaling.

3.11 Stochastic network model with time-dependent coupling and drifting frequencies

The organization of mitochondrial networks in cardiac myocytes as well as the network's inherent topological and dynamical organization have been the subject of previous studies [70,102,103,104]. Since mitochondrial $\Delta\Psi_m$ oscillations exhibit dynamically changing frequencies, the Kuramoto model has been extended to include

frequencies which drift in time. This can be done by introducing a second time scale $1/\gamma$, γ being a measure of the stability of the phase oscillator [79], to model frequency dynamics as Ornstein-Uhlenbeck processes [78,79] (see Table 3.2). Ornstein-Uhlenbeck processes are the prototype of a noisy relaxation process that, for each current frequency value, reverts towards a given mean frequency [80]. They are frequently used in cellular networks where period variability is expected to be correlated in time [79,92,93].

$$\frac{d\varphi_m(t)}{dt} = \omega_m(t) + K_m(t) \sum_{j_m \in N_m} \sin\left(2\pi(\varphi_{j_m}(t) - \varphi_m(t))\right)$$

$$\frac{d\omega_m}{dt} = -\gamma(\omega_m - \mu_m) + \eta_m(t)$$

$$s(t) = \frac{1}{M} \sum_m \cos\left(\varphi_m\right)$$

Symbol	Description
$\varphi_m(t)$	Phase for mito *m*
$\omega_m(t)$	Intrinsic frequency for mito *m*
$\mu_m(t)$	Mean circadian frequency for mito *m*
σ_m	Frequency dispersion for mito *m*
γ	Frequency relaxation rate
$\eta_m(t)$	White noise source with variance σ_η^2
$K_m(t)$	Coupling constant for mito m
$s(t)$	Normalized intensity signal for mito *m*

Table 3.2 Stochastic phase model with drifting frequencies and time-dependent local mitochondrial coupling. (A) An extended Kuramoto model for the oscillator phases $\varphi_m(t)$ and frequencies $\omega_m(t)$ describes coupled circadian phase oscillators. N_m is the total number of nearest neighbors of mitochondrion m. The sum of the coupling term runs over all nearest neighbors j_m of mitochondrion m. The total luminescence signal $s(t)$ is the sum of a population of all oscillators contributing an amplitude-normalized cosine signal. m is the total number of mitochondrial oscillators and the sum of cosines runs over all mitochondrial oscillators. (B) Parameter listing. $K_m(t)$ represents the time-dependent local mitochondrial phase coupling constant.

As a matter of fact, temporal coherence of mitochondrial $\Delta\Psi_m$ recordings has

been observed and quantified recently [59,105]. In Ornstein-Uhlenbeck processes, the frequency dispersion σ_m is a measure of frequency noise, whereas γ is a measure of the intrinsic frequency to adhere to a fixed frequency μ_m, thus revealing the stability of the oscillator (cf. [94]). Variation of γ follows exponential dynamics (Table 3.2): large γ yield intrinsic frequencies that are more dependent on the Gaussian white noise term and thus show a stronger drift than those with small γ [79,106].

In addition to dynamically changing intrinsic frequencies, phase coupling was assumed to underlie dynamical changes as well, to be unique for each mitochondrion and, for each mitochondrion and its nearest neighbors, to be of local mean field type. Each mitochondrion's wavelet frequency was determined according to protocols detailed above and each mitochondrion's frequency fluctuation amplitude σ_m was taken as the standard variation of the measured mitochondrial wavelet frequency. Moreover, the mean frequency towards which the intrinsic frequencies drift in time was taken as the time-dependent mitochondrial wavelet frequency, thus leaving only the decay rate parameter γ fixed for all mitochondria in a cardiac myocyte.

3.11.1 *Decay rate parameter* γ

Each cell's γ was optimized for the forward modeled whole cell TMRE signal to fit the amplitude-normalized experimental whole cell TMRE signal (Figures 3.16-17). For each of the substrate-treated cell groups, mean decay rate parameters were determined to be 7.13e-2 ± 1.55e-2 and 6.46e-2 ± 1.14e-2 for glucose and β-hydroxy-butyrate, respectively, whereas pyruvate and lactate showed slightly smaller decay rate parameters: 6.10e-2 ± 1.26e-2 and 6.29e-2 ± 1.17e-2, respectively (Figure 3.17).

3.11.2 *Spatio-temporal properties of local coupling in mitochondrial frequency clusters*

Time-dependent coupling constants for each mitochondrion in all cardiac myocytes across different substrate groups were determined using the respective optimal decay rate parameters. Cluster and non-cluster mitochondria for each cell were determined as detailed above and, for each recorded point in time, coupling constants were averaged for cluster and non-cluster mitochondria, respectively, to evaluate their respective coupling constants' time evolution (Figure 3.18). To compare myocytes with unequal duration of recordings, each cell's duration of oscillations was set to 1. One

observes higher coupling strengths for cluster mitochondria in cardiac myocytes perfused with glucose and β-hydroxy-butyrate, whereas differences in averaged coupling constants for cluster and non-cluster mitochondria in pyruvate and lactate are less pronounced. Averaging over time yields a mean coupling constant of 7.78e-2 ± 0.98e-2 for cluster and 4.40e-2 ± 0.64e-2 for non-cluster mitochondria, respectively, in glucose-perfused isolated cardiac myocytes. Pyruvate perfusion gave a similar time-averaged mean coupling constant for cluster mitochondria (7.49e-2 ± 1.65e-2), whereas lactate and β-hydroxy-butyrate were found to have lower time-averaged cluster coupling constants (4.83e-2 ± 1.25e-2 and 4.11e-2 ± 0.62e-2, respectively). However, averaged coupling constants for non-cluster mitochondria gave 6.56e-2 ± 1.60e-2, 4.24e-2 ± 1.10e-2 and 2.49e-2 ± 0.34e-2 for pyruvate, lactate and β-hydroxy-butyrate, respectively. For pyruvate and lactate, lower ratios of averaged coupling constants for cluster to non-cluster mitochondria suggest similar spatio-temporal contiguity properties of the

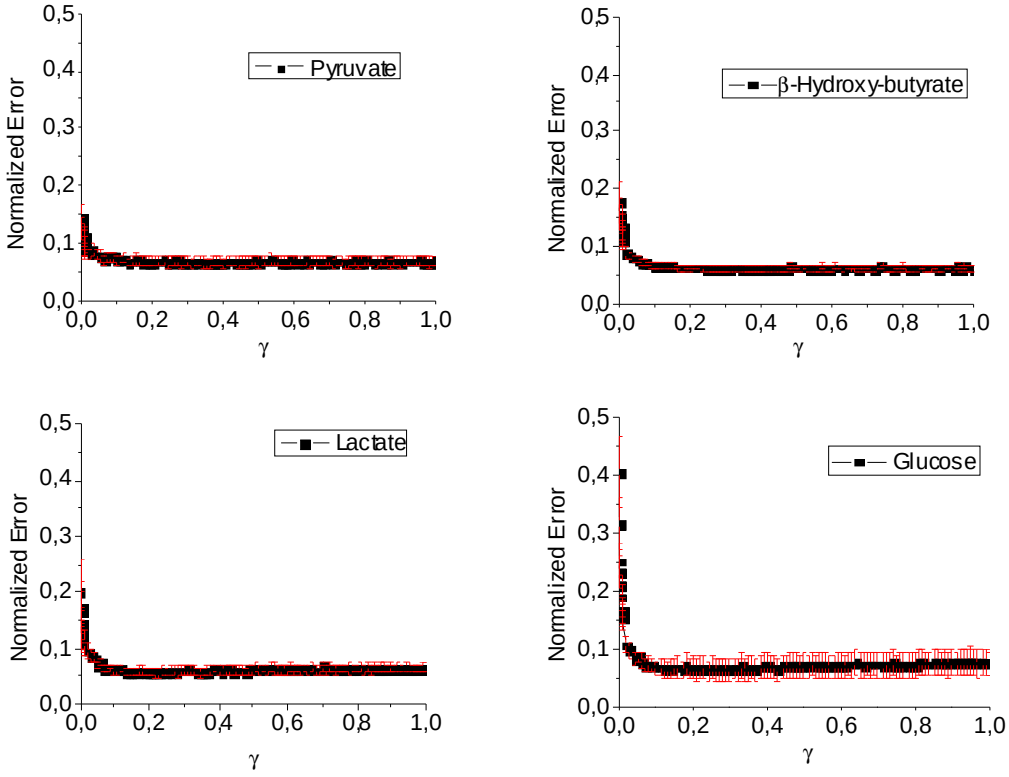

Figure 3.16 Minimum error estimation of decay rate parameter γ in the interval [0,1] for glucose, pyruvate, lactate and β-hydroxy-butyrate respectively. Normalized error versus decay rate parameter γ for all cells with perfusion in glucose (N=9), pyruvate (N=10), lactate (N=7) and β -hydroxy-butyrate (N=14) respectively. Standard errors in red.

mitochondrial clusters. This contiguity might underlie other metabolic control mechanisms as in glucose or β-hydroxy-butyrate and seems to be consistent with the clusters coherence properties (Figure 3.14).

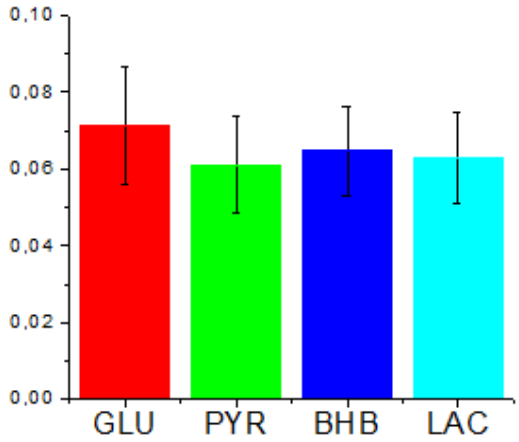

Figure 3.17 Minimum error estimation of decay rate parameter γ in the interval [0,1]. Values of the optimal decay rate parameters for glucose- (GLU), pyruvate- (PYR), lactate- (LAC) and β-hydroxy-butyrate- (BHB) perfused cardiac myocytes (the γ distributions are not significantly different to each other (one-way analysis of variance: F-value = 0.14, P-value = 0.9366).

To further explore effects of inter-mitochondrial coupling on the mitochondrial network organization, mitochondrial mean cluster coupling constants were plotted versus % cluster area and mean cluster frequency for each point in time (Fig. 3.19-20). As detailed above, time-dependent cluster affiliation for mitochondria had been determined according to dynamic mitochondrial frequency behavior and not physical proximity. Therefore, a quantification of inter-mitochondrial coupling for local environments with nearest-neighbor-coupling was not thought to be necessarily connected to temporal cluster organization since, so far, coupling has been thought of a diffusive process with ROS as molecular coupling agents [22,107]. Nevertheless, linear polynomial fitting yielded a slightly ascending linear function for cluster coupling versus % cluster area with a slope of 2.04e-2 ± 0.53e-2 [1/%] for glucose-perfused myocytes (Figure 3.19). This tendency could be confirmed for perfusion of cells with lactate (4.98e-2 ± 0.30e-2 [1/%]) and pyruvate (4.63e-2 [1/%] ± 0.54e-2 [1/%]). Here, inter-mitochondrial coupling grows with % cluster size, indicating an overall increase in coupling strength for nearest-neighbor coupling towards synchronization of the whole

network. However, β-hydroxy-butyrate-perfused cardiac myocytes were found to give a descending slope (-4.70e-2 ± 0.20e-2 [1/%]).

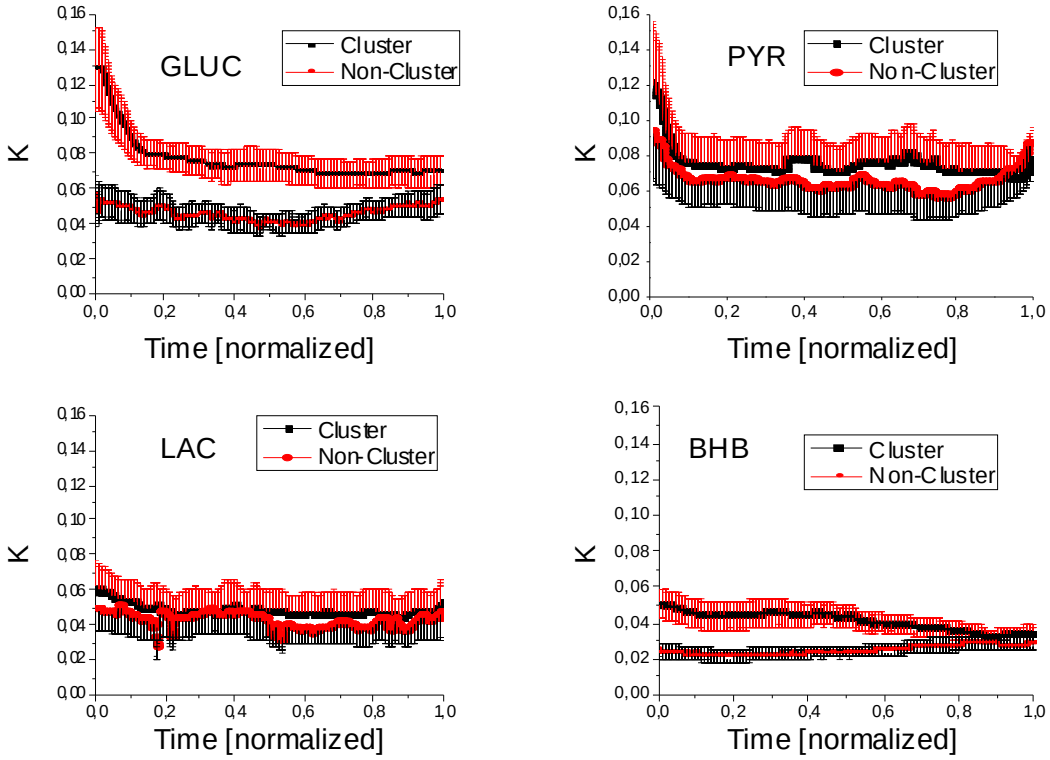

Figure 3.18 Mean mitochondrial cluster constants versus mean non-cluster. Averaged coupling constants for each point in time for perfusion with pyruvate, β-hydroxy-butyrate, lactate and glucose respectively. To allow the statistical comparison among myocytes with unequal recording durations, the duration of the oscillations of each recording was normalized. For pyruvate and lactate, lower ratios of averaged coupling constants for cluster to non-cluster mitochondria suggest similar spatio-temporal contiguity properties of the mitochondrial clusters. This contiguity might underlie other metabolic control mechanisms as in glucose or β-hydroxy-butyrate and seems to be consistent with the clusters' coherence properties (Fig. 3.14). K-value distributions were compared across substrates for cluster and non-cluster mitochondria and all found to be significantly different to each other ($p < 0.05$).

This difference towards the other substrates indicates altered organizational principles of the mitochondrial network that seem to be governed by metabolic effects of β-oxidation on the mediation of inter-mitochondrial coupling [108]. In contrast, linear regression on mitochondrial mean cluster coupling constants versus mean mitochondrial cluster frequency gave an ascending linear fit across the different substrates (Figure 3.20) with similar slopes of 3.31e-3 [1/mHz] ± 0.1e-3 [1/mHz], 3.14e-

3 ± 0.03e-3 [1/mHz], 4.01e-3 ± 0.09e-3 [1/mHz] and 3.07e-3 ± 0.04e-3 [1/mHz] for cell-perfusion with glucose, pyruvate, lactate and β-hydroxy-butyrate, respectively. The results indicate that local nearest-neighbor coupling for cluster mitochondria is strongest for cluster mitochondria that oscillate at higher frequencies.

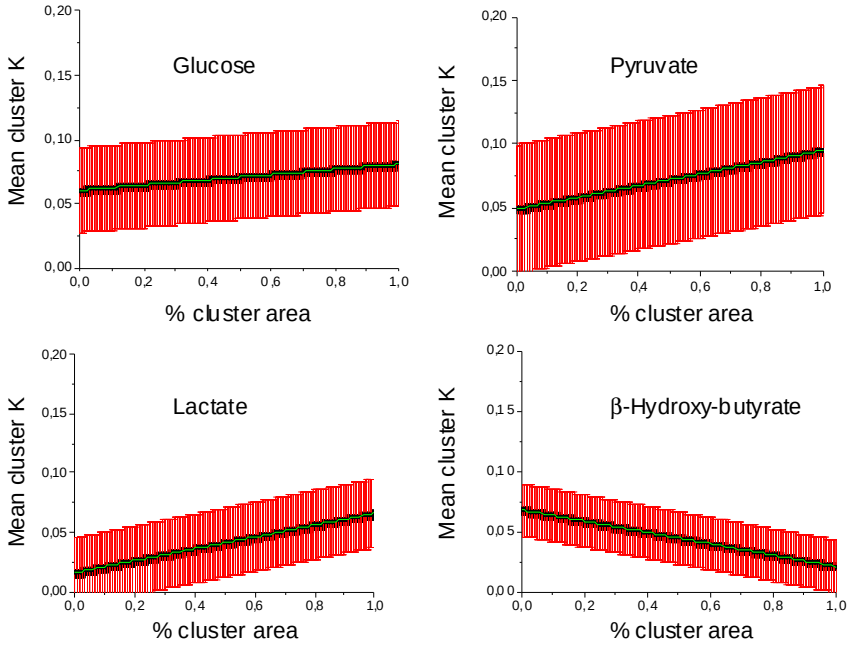

Figure 3.19 Mitochondrial network intrinsic cluster coupling versus % cluster area. Linear fit with standard errors (red) of mean mitochondrial cluster constant versus % cluster area for each point in time across all substrates. For glucose, pyruvate and lactate, inter-mitochondrial coupling grows with % cluster size, indicating an overall increase in coupling strength for nearest-neighbor coupling towards synchronization of the whole network. β-hydroxy-butyrate-perfused cardiac myocytes, however, seem to be governed by metabolic effects of β-oxidation on the mediation of inter-mitochondrial coupling.

3.11.3 *Forward model and model validity*

Forward modeling for whole-cell intensity signals with cell-specific optimal decay parameter γ and corresponding mitochondrial coupling constants was done by cross-correlating the cosine of the whole-cell TMRE signal wavelet phase and the sum of cosines of the forward modeled phases of the stochastic model (Figure 3.21). High correlation coefficients indicate the similarity of predicted signals and the real data signal, providing validity for the acquired coupling constants. Correlation coefficients for each cardiac myocyte were determined to be 0.88 ± 0.02, 0.64 ± 0.05, 0.85 ± 0.03 and

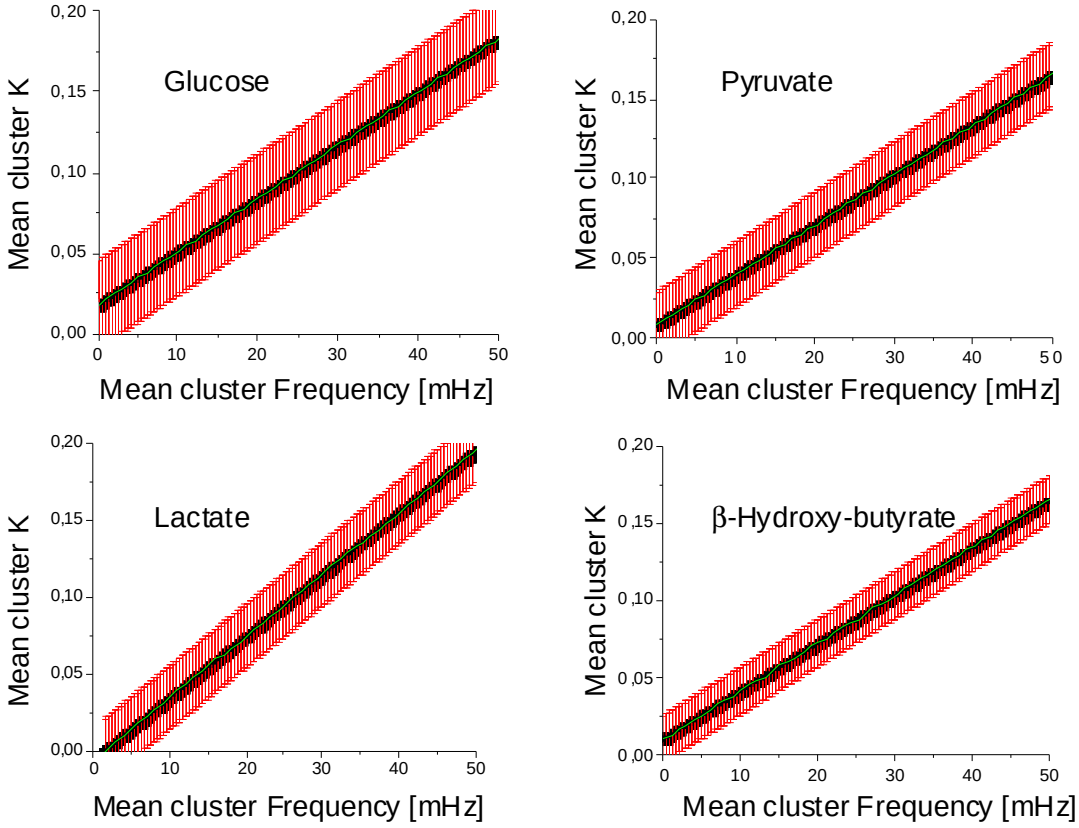

Figure 3.20 Mitochondrial network intrinsic cluster coupling versus mean cluster frequency. Linear fit with standard errors of mean mitochondrial cluster coupling constant versus mean mitochondrial cluster frequency for each point in time. Across all substrates, higher frequencies are positively correlated with strong local nearest-neighbor coupling.

0.75 ± 0.03 for glucose-, pyruvate-, lactate- and β-hydroxy-butyrate-treated myocytes, respectively (Figure 3.22).

Smaller correlation coefficients for forward-modeled pyruvate-perfused cardiac myocytes imply that the applicability of stochastic mitochondrial phase modeling has limitations for cardiac myocytes with both a high degree of frequency dispersion and a low degree of cluster contiguity. This problem could be partly circumvented by only focusing on those 10 cluster mitochondria with the highest averaged signal cross-correlation to their nearest neighbors: here, cluster contiguity is most likely ensured.

Subsequent cross-correlation of the cluster ensemble's individual cosine of the forward modeled phase signals with that of the cosine of the ensemble's wavelet phase gave correlation coefficients of 0.95 ± 0.02, 0.81 ± 0.04, 0.88 ± 0.05 and 0.86 ± 0.02 for glucose-, pyruvate-, lactate- and β-hydroxy-butyrate-perfused myocytes, respectively

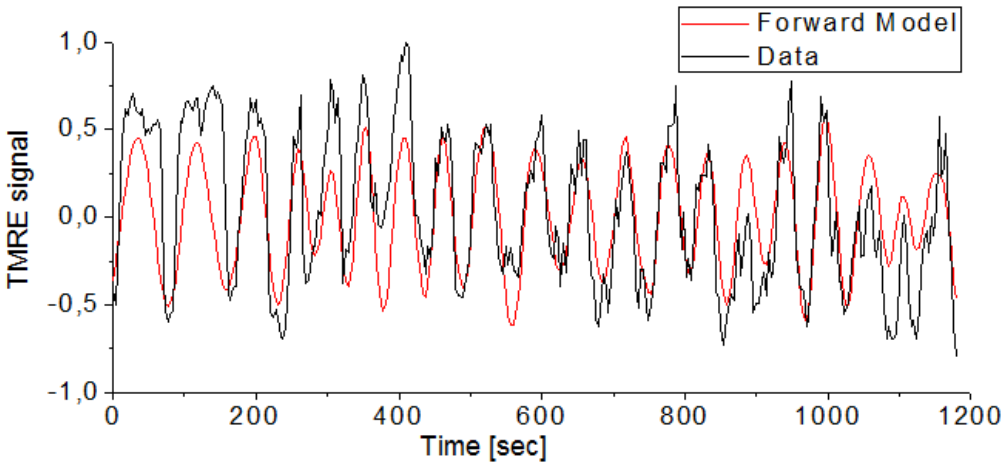

Figure 3.21 Forward modeling with optimal decay rate parameter γ. (A) Intensity normalized real data for a lactate-perfused myocyte (black). The TMRE signal has been subtracted by its median value and the corresponding signal was normalized to its maximum value. Forward modeled cosine phase signals from all mitochondria (red).

(Figure 3.21). Thus, for contiguous cluster ensembles, the model's output signal is highly correlated with the real data signal across all substrates.

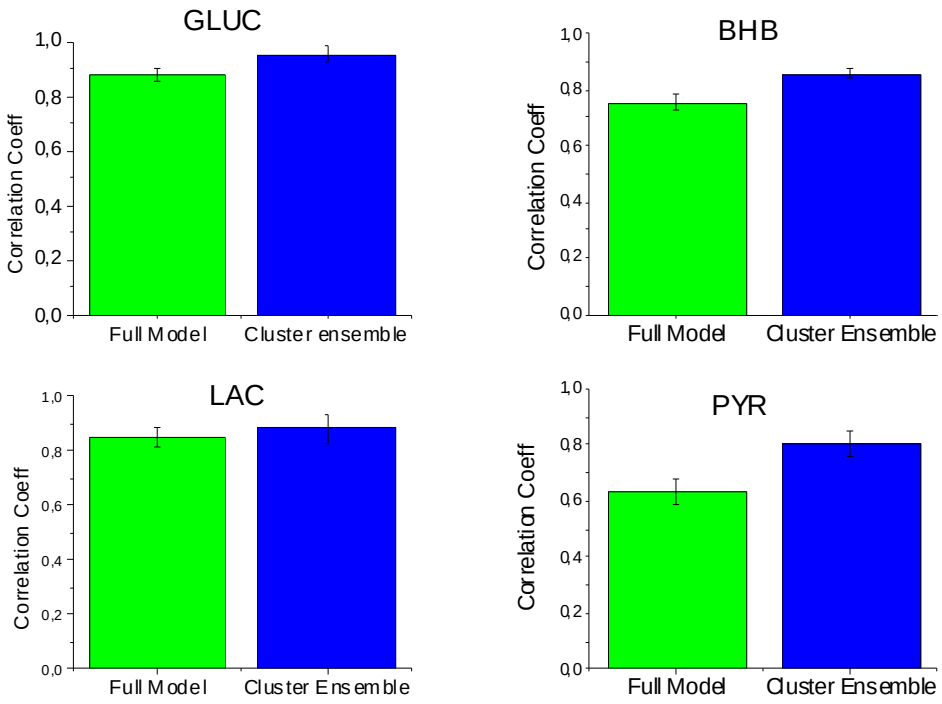

Figure 3.22 Model validity. Cross-correlation coefficients for forward modeled signal to the cosine of the wavelet-determined phase of the whole cell signal (right-hand side of each panel). Smaller correlation coefficients of pyruvate-perfused cardiac myocytes reveal limitations of the stochastic mitochondrial phase model for cardiac myocytes with both a high degree of frequency dispersion and a low degree of cluster contiguity. Only considering the 10 cluster mitochondria with the highest averaged signal cross-correlation to their nearest neighbors (left-hand side of each panel) yields correlation coefficients close to 1 since cluster contiguity is most likely ensured.

IV Discussion

Under oxidative stress, the imbalance between ROS generation and ROS scavenging of individual cardiac mitochondria results in a destabilization of $\Delta\Psi_m$ for a significant portion of the mitochondrial network (~60%) [36], which forces the network to oscillate synchronously. The proposition of the presence of individual mitochondrial oscillators considers that these oscillators are weakly coupled in the physiological state, when ROS levels are low, and are strongly coupled in the pathophysiological state, when ROS levels are high. This transition has a profound impact on myocyte electrical excitability and intracellular calcium handling [27] and has been implicated in post-ischemic dysfunction of the heart [47]. The proposed coupling mechanism that involves RIRR [29] and is mediated by ROS diffusion has recently received further experimental and theoretical support [73].

4.1 Heterogeneous time-dependent oscillations of individual mitochondria

4.2 Spatio-temporal organization of mitochondrial frequency clusters

Instead of selecting spanning clusters using a ROS level threshold [22], the focus was put on major clusters of mitochondria to find the relationship between frequency and amplitude of oscillation or the actual size of the cluster. This procedure allowed to uniquely identify closely connected clusters by their main frequency component, whilst still taking into account smaller clusters with different frequencies. The mitochondria are therefore grouped into clusters solely by examining their frequencies in a narrow range, at a specific point in time, and should not be thought of as morphologically connected clusters.

In fact, cardiac myocytes possess mitochondria that may show static (morphology and biochemical properties) and dynamic heterogeneity. Static morphological distinctions include mitochondria in intermyofibrillar locations, subsarcolemmal mitochondria and perinuclear mitochondria [40,41]. It has also been suggested that these differentially localized mitochondria may have different functional properties [43,44].

These spatio-temporally organized networks underlie complex control mechanisms that influence oxidative phosphorylation and possibly lead to emergent macroscopic responses. Dynamic heterogeneity becomes especially significant under metabolic [28] or oxidative stress and the scaling of network instabilities to whole myocyte and even whole organ function has been recently examined [36,46,47,48]. In these studies, it was shown that mitochondrial criticality, i.e., the abrupt and synchronous collapse of $\Delta\Psi_m$ in individual cells or clusters of cells during ischemia-reperfusion injury, can contribute to the generation of fatal ventricular arrhythmias.

Recently, application of network theory on mitochondrial networks has helped to understand the functional connectivity of mitochondria [103], especially the concept of scale-free mitochondrial networks [22,36,59,105]. Self-similar, fractal mitochondrial network behavior could be demonstrated with relative dispersional analysis and power spectral analysis for cardiac myocytes, but was also found to be applicable to S. cerevisiae mitochondria (reviewed in [102]). Qualitatively, wavelet analysis of S. cerevisiae beautifully demonstrates the intricate frequency pattern in yeast that explicates different scale components of the signal as predicted by fractal dynamics (see Figure 4.1).

These studies have provided evidence that mitochondrial morphology is linked to function (for example, in the case of coupling between mitochondria and the L-type calcium channel [45]) and that changes in metabolic fluxes may occur by altering the structure of the mitochondrial network and/or the topology of the mitochondrial membranes, which may be structural organizing centers for several intracellular signaling pathways (reviewed in [2,109]).

Some authors support the concept of a single reticular mitochondrial network that replaces the classical mitochondrion organelle [110]. In this model mitochondria are unipotential, therefore synchronization of oscillations with different mitochondrial frequency spectra would not be possible. Thus, the findings of the present work don't

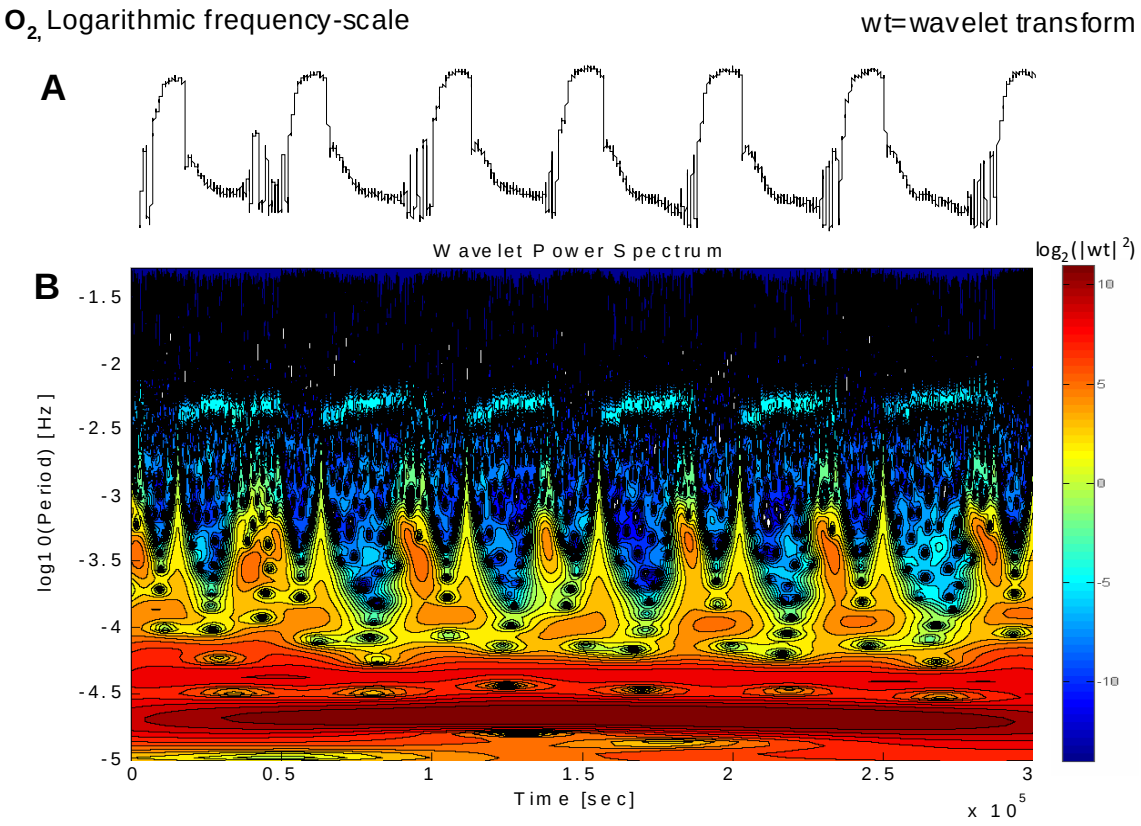

Figure 4.1 Wavelet analysis of the O_2 signal time series obtained from the self-organized multi-oscillatory continuous culture of S. cerevisiae. (A) Relative membrane inlet mass spectrometric signal of O_2 versus time for S. cerevisiae. The time scale is not shown, but corresponds to hours after the start of continuous fermentor operation. Large-amplitude oscillations show substantial cycle-to-cycle variability with 13.6 ± 1.3 h (N=8). Other evident oscillation periods are ~40 min and ~4 min. This figure was provided courtesy of Prof. David Lloyd, affiliated with Cardiff University, United Kingdom. (B) Logarithmic absolute squared wavelet transform over logarithmic frequency and time. At any time, the wavelet transform uncovers the predominant frequencies and reveals a complex and fine dynamic structure that is associated with mitochondrial fractal dynamics. Boxes and arrows show the correspondence between the time series and the wavelet plot.

support this concept of mitochondrial reticulum but are best understood with the classical view on mitochondrial structure. It has also been shown that individual mitochondria can respond independently of the network [29], [24,111,112].

In that context, observations of complete or chaotic synchronization [113,114,115] support the idea that cluster partitioning in networks of coupled oscillators can take place; the network splits into several clusters of mutually synchronized oscillators [116]. In addition, a model employing gradient coupling [117] exemplifies that around an optimal gradient, most oscillators can be synchronized to the same frequency,

indicating a higher system coherence. Additionally, oscillators for large gradient coupling can be divided into synchronized clusters with different frequencies while still maintaining high system coherence.

It should be noted that mitochondrial coupling that starts from a nucleus of excited mitochondria (cf. [22]) is not an instantaneous process, but rather occurs in a finite time interval through diffusion mediated processes within the coupling medium. Thus, this process appears to take more time to evolve in larger clusters and hence in such case full synchronization of all mitochondria requires more time (Figure 3.5). This effect alone leads to prolonged cluster depolarization and therefore lower cluster frequency. Alternatively, one may arrive at the same conclusion by considering the more general theory which suggests that the frequency and phase of coupled oscillators adjusts to a common mode, and that the larger the clusters the longer it takes to synchronize as a group [100,101].

4.3 Mitochondrial cluster organization in the intact heart

Within the pathophysiological regime of cardiac myocytes, the wavelet-based signaling tools and characterization methods of individual mitochondrial $\Delta\Psi_m$ oscillations were applied to uncover significant correlations of the size of a cluster of similarly oscillating mitochondria and their mean frequency for functionally intact slices of ventricular heart tissue with connected ventricular myocytes.

Stress-induced mitochondrial $\Delta\Psi_m$ oscillations have previously been shown to occur not only for isolated cardiac myocytes but also for intact hearts perfused with solutions containing glucose [83]. Although the triggering of $\Delta\Psi_m$ depolarization within cells of the myocardial syncytium was reported to be more resistant than for isolated myocytes, the findings generalized former results for single cardiac myocytes [29,36] and computational modeling for the intact heart [71,118]. Here, it was pointed out that mitochondrial collective behavior for clusters of mitochondria with similar frequencies seems to be analogous to that in isolated cardiomyocytes. This indicates that metabolic, molecular and electrical communication via gap junctions between cardiac myocytes does not significantly modify mitochondrial network dynamics under stress. In fact, RIRR mechanisms within myocytes of the myocardial syncytium have been found to be consistent with those in isolated cardiac myocytes [83]. Depolarizations within myocytes of the intact heart have been observed to be partly spontaneous in some cardiac

myocytes after laser-flashing of neighboring cells, thus indicating relay properties for mitochondrial coupling agents at inter-cellular junctions. Moreover, mitochondrial cluster organization seemed to be limited to smaller fractions of the cell than those observed in isolated cardiac myocytes. In line with a reported stronger resistance towards network synchronization after laser-flashing [83], this could indicate weaker inter-mitochondrial coupling due to either more pronounced, possibly inter-cellularly communicated ROS scavenging capacities or for the same reason a significantly different functionality of the networks' boundary mitochondria in the proximity of gap junctions. However, similar dynamic network properties of myocardial syncytium and isolated myocytes might provide further affirmation for future therapeutic interventions with mitochondrial benzodiazepine ligands or inhibition of mitochondrial ROS production [29,118] to prevent post-ischemic dysfunction of the whole heart.

4.4 Substrate specificity of mitochondrial cluster dynamics

Apart from glucose, oxidative phosphorylation in heart cells can be increased by other energy suppliers whose degradation pathways end in substrates that are fed to the Krebs cycle [1,82]. Substrates for the Krebs cycle consumed from β-oxidation in cells of the intact heart make up for about 50% to almost 100% of the substrates [1,108] whereas substrates from glycolysis only account for about 30% and the remaining substrates are provided by lactate and amino acids [1]. Here, this has been found to be reflected in the strength of correlation between mitochondrial % cluster size and mean cluster frequency: cardiac myocytes perfused with β-hydroxy-butyrate demonstrated the strongest change in % cluster size vs. mean cluster frequency. Also, mitochondrial frequencies were found to be within a more narrow low-frequency range as compared to the other substrates. Naturally, in the presence of increased ROS, inter-mitochondrial coupling through RIRR mechanisms is thought to manifest more thoroughly. Therefore, dynamic mitochondrial clusters would form more rapidly by recruiting other mitochondrial oscillators which in turn would leave fewer clusters with different frequencies, i.e. narrowing the mitochondrial frequency distribution.

Cardiac myocytes perfused with pyruvate, the end product of glycolysis and also of the degradation of all smaller amino acids, exhibit a high rate of conversion to lactate under oxidative stress [119]. This leads to low pH-levels and a decrease in contractility via increased ATP demand for the sarcoplasmic calcium pump and for regulation of

calcium homeostasis [119,120]. Pyruvate is known to suppress cytosolic NADH oxidase activity, therefore inhibiting extramitochondrial ROS formation [119]. However, a significant amount of pyruvate in mitochondria is still assumed to be processed by the pyruvate dehydrogenase to yield acetyl-CoA for the Krebs cycle [1], in general more than for glucose, the starting point of glycolysis. This was indeed found to be reflected in a 35% increase of the rate of change of % cluster area versus cluster frequency, however, the mitochondrial frequency distribution appeared larger than that for other substrates. Also, pyruvate-perfused cardiomyocytes were found to possess almost similar coherence values in cluster and non-cluster mitochondria and observed to show a higher degree of non-contiguity than cells in other substrate groups.

Taken together, the findings indicate that mitochondrial network synchronization in pyruvate, other than in β-hydroxy-butyrate, first occurs in several small clusters throughout the cell. The finding relate to the problem of synchronization: higher slope and larger frequency distribution represent a signature of desynchronization due to dynamic heterogeneity. The model presented herein attributes this fundamental feature to time-dependent drifting frequencies of the oscillators. Mechanistically, time-dependent drifting frequencies can be explained by local dynamics of ROS production and ROS scavenging systems involving mitochondrial matrix and the extra-mitochondrial compartment [121]. Interestingly, the two substrates leading to the most reduced redox potential, pyruvate and β-hydroxybutyrate, have higher % area of the cluster. However, β-hydroxybutyrate-perfused cardiac myocytes do not increase in coupling constant proportion for higher frequencies. This may indicate the influence of additional redox processes or metabolic effects, respectively, on mitochondrial cluster formation.

Metabolically, the major difference between pyruvate and lactate is that cytosolic NADH/NAD^+ redox potential is pegged either in the fully oxidized (pyruvate) or fully reduced (lactate) states and both would likely lead to more reduced matrix NADH than in glucose, feeding NADH oxidase. This would concur with an increase in ROS production and hence higher inter-mitochondrial coupling rates. In the model, this is true for pyruvate, where mean coupling is higher than for glucose (Figure 3.18). However, mean coupling for lactate is lower than for glucose, thus indicating more complex redox relations. Additional studies will be required to determine the exact role of ROS in substrate-dependent redox processes and therefore mitochondrial network behavior.

Finally, lactate in cardiac myocytes is oxidized to pyruvate and then, in the presence of oxygen, directly used to fuel the Krebs cycle [1]. It could be shown that lactate contributes significantly to acetyl-CoA formation, often more than glucose [122,123,124]. An increase in lactate density counteracts the degradation of pyruvate to lactate under oxidative stress, and induces an increase in ROS formation [119]. There are studies attributing signaling properties to lactate anions via lactate-responsive genes, however, effects were reported to take place at least 1 hour after beginning of measurements [125]. Here, glucose- and lactate-perfused cardiomyocytes were found to have a similar rate of change of % cluster area versus cluster frequency, whereas frequencies for lactate perfusions were in general slightly lower. Since mitochondrial cluster coherence in lactate-perfused cardiac myocytes was observed to be less pronounced to non-cluster coherence than for glucose perfusion, these results point to a higher degree of cluster non-contiguity and/or lower signal correlation of mitochondria with similar frequencies.

4.5 Dynamic mitochondrial coupling

A stochastic model was proposed that provides a measure of stability of mitochondrial phase oscillators across four differently substrate-perfused cardiac myocytes and mathematically visualizes the role of inter-mitochondrial coupling by providing time-dependent individual mitochondrial coupling constants. In addition, correlations between mean mitochondrial cluster coupling and % cluster size as well as mean cluster frequency are revealed.

The concept of scale-free mitochondrial networks has been introduced recently to describe inter-mitochondrial coupling across different spatio-temporal domains in cardiac myocytes [22,59,70]. Weak temporal organization under physiological conditions is strengthened in the pathophysiological regime where the mitochondrial oscillators mostly lock in low-frequency and large amplitude oscillations [22,47]. In this regard, cardiac mitochondria, like yeast, have been proposed to possess inherent characteristics of a biological clock [59,126,127]. Mathematical descriptions of the transition of such multiple oscillator networks to synchrony have been addressed by several authors (see for example [62,63,64,65]). These studies show that coupling starting in a synchronized nucleus of excited oscillators can recruit new oscillators until a critical mass of oscillators induces spontaneous self-synchronization across the network [22,64]. The introduction of time-drifting frequencies to model circadian network

behavior as an extended Kuramoto model with intrinsic Ornstein-Uhlenbeck frequencies [78,79] closely applies to mitochondrial frequency dynamics. This is because, in cardiac myocytes, mitochondrial phase dynamics is subject to diffusion-mediated inter-mitochondrial coupling processes [22,70]: coupling agents such as ROS locally keep information about the mitochondrion's oscillatory behavior through the inertness of ROS density changes in the diffusive medium, attributing an inherent frequency stiffness towards the actual mitochondrial frequency for each individual mitochondrial oscillator.

Frequency drifts are governed by the value of the decay rate parameter γ; at a fixed frequency dispersion of the mitochondrial network, the collective groups into distinct locked and incoherent clusters whose formation depends on the proximity of individual frequencies to each other [78]. On the other hand, large decay rate parameters decrease the frequency distribution and contribute to equalization of dynamic cluster properties [78,79]. Therefore, the results for the decay rate parameter indicates that cardiac myocytes perfused with substrates like pyruvate and lactate, which possess slightly smaller decay rate parameters than glucose or β-hydroxy-butyrate, show, to some extent, a greater variety of frequency-locked clusters. Even though the differences are not significant, this would be consistent with the notion of similar temporal coherence properties of the major frequency cluster and non-cluster mitochondria for pyruvate and lactate and also with spatio-temporal cluster properties that are derived from the relation of % cluster area and mean cluster frequency. Also, lower ratios of averaged coupling constants for cluster to non-cluster mitochondria in pyruvate- and lactate-perfused cardiomyocytes (Figure 3.18) indicate differences of cluster contiguity and frequency dispersion towards glucose- and β-hydroxy-butyrate-perfusion.

Nevertheless, the significant correlation observed between mean cluster frequency and mean cluster coupling constant seems universally true across all examined cell perfusions. Mitochondrial RIRR adds to basal ROS concentrations and significantly increases local ROS density for small areas of highly contiguous phase-locked mitochondrial oscillators [128]. Since growing clusters lose contiguity and their mean frequency decreases (Figures 3.10-13, 3.15), i.e. the frequency of local ROS sparks reduces, ROS densities in nearest-neighbor environments also decrease, resulting in a decrease of inter-mitochondrial coupling (Figure 3.20). However, formation of cell-wide spanning clusters [22,36] slightly increases overall basal ROS concentration,

as a result of which local inter-mitochondrial coupling slightly increases as well (Figure 3.19).

The results suggest that the correlation between local mitochondrial coupling and mitochondrial cluster frequency is mainly driven by early cluster formation where the averaged coupling constant is mildly (β-hydroxy-butyrate and lactate) to strongly (glucose and pyruvate) higher (cf. Figure 3.18) than for the rest of the recording. Local coupling and % cluster area are, on the other hand, mostly determined through low coupling constants at the end of the recordings where most mitochondria have been integrated into the spanning cluster and cytosolic ROS density increases with % cluster area. However, the observed negative correlation of local inter-mitochondrial coupling with % cluster area for β-hydroxy-butyrate-perfused cardiac myocytes implies that other local coupling mechanisms have to be taken into account. For example, under oxidative stress, alterations in β-oxidation promote mitochondrial functionality changes through accumulation of acyl carnitine and acyl CoA esters [108].

4.6 Conclusion

In summary, in this work a wavelet-based method to characterize the temporal organization of individual mitochondrial oscillations of a heterogeneous mitochondrial network in the pathophysiological regime is presented. This approach of identifying individual mitochondria and assigning to their respective fluorescence intensity a time-dependent frequency is an essential tool in examining the spatio-temporal characteristics of a network of coupled mitochondrial oscillators, such as coupling, coherence and synchronization properties. It provides the possibility to quantitatively study an intracellular network with methods of network and synchronization analysis and provides the basis for the subsequently developed stochastic model of mitochondrial network behavior.

Moreover, the present work shows that % cluster area is inversely correlated with cluster mean frequency. Apart from glucose-perfused isolated cardiac myocytes, this relation could also be confirmed for cell perfusion with pyruvate, lactate and β-hydroxy-butyrate as well as for connected cells in the intact heart. The results therefore underline the universality of this correlation that reflects the importance of spatial and temporal organization on network functionality. They elucidate cardiac myocyte behavior near death: the dying myocyte loses $\Delta\Psi_m$ as the mitochondrial clusters grow

larger, and the energetic and antioxidant deficiencies grow until recovery of the network is impossible.

Additionally, during synchronized oscillations it is shown that, for glucose-perfused cardiac myocytes, the % cluster size is inversely correlated with the % amplitude within the pathophysiological regime, which actually reflects the failure of the network to completely repolarize between oscillations (Figure 3.7B). Also, mitochondrial nearest neighbor coupling is demonstrated to be strongly influenced by the organization of mitochondria along the myofilaments.

Furthermore, the present work quantifies inter-mitochondrial coupling by introducing a stochastic phase model that can be used to examine mitochondrial network dynamics and that provides insights into mitochondrial network topology under different metabolic conditions. The findings highlight the importance of both spatial and temporal organization in defining how the mitochondrial network functions.

V. References

1. Lehninger A, Nelson DL, Cox MM. Lehninger Principles of Biochemistry: W. H. Freeman, 2008.
2. McBride HM, Neuspiel M, Wasiak S. Mitochondria: more than just a powerhouse. Curr Biol 2006;16(14):R551-560.
3. Alberts B, Bray D, Lewis J, et al. Molecular Biology of the cell. New York: Garland Science, 1995.
4. Dorn GW. Mitochondrial dynamics in heart disease. Biochim Biophys Acta 2012:doi:10.1016/j.bbamcr.2012.1003.1008.
5. Lardy HA, Wellman H. Oxidative phosphorylations; role of inorganic phosphate and acceptor systems in control of metabolic rates. J Biol Chem 1952;195:215-224.
6. Katz LA, Swain JA, Portman MA, et al. Relation between phosphate metabolites and oxygen consumption of heart in vivo. Am J Physiol 1989;256:H265-H274.
7. Balaban RS, Kantor HL, Katz LA, et al. Relation between work and phosphate metabolite in the in vivo paced mammalian heart. Science 1986;232:1121-1123.
8. Cortassa S, Aon MA, Marban E, et al. An integrated model of cardiac mitochondrial energy metabolism and calcium dynamics. Biophys J 2003;84(4):2734-2755.
9. Maack C, Cortassa S, Aon MA, et al. Elevated cytosolic Na+ decreases mitochondrial Ca2+ uptake during excitation-contraction coupling and impairs energetic adaptation in cardiac myocytes. Circ Res 2006;99(2):172-182.
10. Denton RM. Regulation of mitochondrial dehydrogenases by calcium ions. Biochim Biophys Acta 2009;1787(11):1309-1316.
11. Ferrari R, Censi S, Mastrorilli F, et al. Prognostic benefits of heart rate reduction in cardiovascular disease. Eur Heart J Suppl 2003;5:G10-G14.
12. Page E, McCallister LP. Quantitative electron microscopic description of heart muscle cells; application to normal, hypertrophied and thyroxin-stimulated hearts. Am J Cardiol 1973;31:172-181.
13. Ruiz-Meana M, Fernandez-Sanz C, Garcia-Dorado D. The SR-mitochondria interaction: a new player in cardiac pathophysiology. Cardiovascular Research 2010;88:30-39.
14. Bers DM. Calcium cycling and signaling in cardiac myocytes. Annu Rev Physiol 2008;70:23-49.
15. Bers DM, Despa S. Cardiac myocytes Ca2+ and Na+ regulation in normal and failing hearts. J Pharmacol Sci 2006;100:315-322.
16. Carafoli E. Calcium pump of the plasma membrane. Physiol Rev 1991;71:129-153.
17. Ruknudin AM, Lakatta EG. The regulation of the Na/Ca exchanger and plasmalemmal Ca2+ ATPase by other protins. Ann NY Acad Sci 2007;1099:86-102.
18. Shull GE, Okunade G, Liu LH, et al. Physiological functions of plasma membrane and intracellular Ca2+ pumps revealed by analysis of null mutants. Ann NY Acad Sci 2003;986:453-460.
19. Maack C, O'Rourke B. Excitation-contraction coupling and mitochondrial energetics. Basic Res Cardiol 2007;102:369-392.
20. Aon MA, Cortassa S, O'Rourke B. Mitochondrial oscillations in physiology and pathophysiology. Adv Exp Med Biol 2008;641:98-117.
21. Aon MA, Cortassa S, Akar FG, et al. Mitochondrial criticality: a new concept at the turning point of life or death. Biochim Biophys Acta 2006;1762(2):232-240.

22. Aon MA, Cortassa S, O'Rourke B. The fundamental organization of cardiac mitochondria as a network of coupled oscillators. Biophys J 2006;91(11):4317-4327.
23. Berns MW, Siemens AE, Walter RJ. Mitochondrial fluorescence patterns in rhodamine 6G-stained myocardial cells in vitro: Analysis by real-time computer video microscopy and laser microspot excitation. Cell Biophys 1984;6(4):263-277.
24. Loew LM, Tuft RA, Carrington W, et al. Imaging in five dimensions: time-dependent membrane potentials in individual mitochondria. Biophys J 1993;65(6):2396-2407.
25. O'Reilly CM, Fogarty KE, Drummond RM, et al. Spontaneous mitochondrial depolarizations are independent of SR Ca2+ release. Biophys J 2003;85(5):3350-3357.
26. Huser J, Rechenmacher CE, Blatter LA. Imaging the permeability pore transition in single mitochondria Biophys J 1998;74(4):2129-2137.
27. O'Rourke BR, B.M., Marban E. Oscillations of Membrane Current and Excitability Driven by Metabolic Oscillations in Heart Cells. Science 1994; 265:962–966.
28. Romashko DN, Marban E, O'Rourke B. Subcellular metabolic transients and mitochondrial redox waves in heart cells. Proc Natl Acad Sci USA 1998;95(4):1618-1623.
29. Aon MA, Cortassa S, Marban E, et al. Synchronized whole cell oscillations in mitochondrial metabolism triggered by a local release of reactive oxygen species in cardiac myocytes. J Biol Chem 2003;278(45):44735-44744.
30. Gooch VD, Packer L. Oscillatory systems in mitochondria. Biochim Biophys Acta 1974;346(34):245-260.
31. Chance B, Yoshioka T. Sustained oscillations of ionic constituents of mitochondria. Arch Biochem Biophys 1966;117:451-465.
32. Evtodienko YV. Sustained oscillations of transmembrane Ca2+ fluxes in mitochondria and their possible biological significance. Membr Cell Biol 2000;14:1-17.
33. Zorov DB, Filburn CR, Klotz LO, et al. Reactive oxygen species (ROS)-induced ROS release: a new phenomenon accompanying induction of the mitochondrial permeability transition in cardiac myocytes. J Exp Med 2000;192:1001 - 1014.
34. Zorov DB, Juhaszova M, Sollot SJ. Mitochondrial ROS-induced ROS release: an update and review. Biochim Biophys Acta 2006;1757:509 - 517.
35. Scaduto RC, Grotyohann LW. Measurement of mitochondrial membrane potential using fluorescent rhodamine derivatives. Biophys J 1999;76(1):469-477.
36. Aon MA, Cortassa S, O'Rourke B. Percolation and criticality in a mitochondrial network. Proc Natl Acad Sci USA 2004;101(13):4447-4452.
37. O'Rourke B. Pathophysiological and protective roles of mitochondrial ion channels. J Physiol 2000;529(1):23-36.
38. Aon MA, Cortassa S, Akar FG, et al. From mitochondrial dynamics to arrhythmias. Int J Biochem Cell Biol 2009;41(10):1940-1948.
39. Brady NR, Elmore SP, van Beek JJ, et al. Coordinated behavior of mitochondria in both space and time: a reactive oxygen species-activated wave of mitochondrial depolarization. Biophys J 2004;87:2022-2034.
40. Kuznetsov AV, Usson Y, Leverve X, et al. Subcellular heterogeneity of mitochondrial function and dysfunction: evidence obtained by confocal imaging. Mol Cell Biochem 2004;256-257(1-2):359-365.
41. Manneschi L, Federico A. Polarographic analyses of subsarcolemmal and intermyofibrillar mitochondria from rat skeletal and cardiac muscle. J Neurol Sci 1995;128(2):151-156.

42. Benda C. Über die Spermatogenese der Vertebraten und höherer Evertebraten, II. Theil: Die Histiogenese der Spermien. Arch Physiol 1898;73:393-398.
43. Kuznetsov AV, Mayboroda O, Kunz D, et al. Functional imaging of mitochondria in saponin-permeabilized mice muscle fibers. J Cell Biol 1998;140(5):1091-1099.
44. Lesnefsky EJ, Tandler B, Ye J, et al. Myocardial ischemia decreases oxidative phosphorylation through cytochrome oxidase in subsarcolemmal mitochondria. Am J Physiol 1997;273(3 Pt 2):H1544-1554.
45. Viola HM, Arthur PG, Hool LC. Evidence for regulation of mitochondrial function by the L-type Ca2+ channel in ventricular myocytes. J Mol Cell Cardiol 2009;46(6):1016-1026.
46. O'Rourke B, Cortassa S, Aon MA. Mitochondrial ion channels: gatekeepers of life and death. Physiology (Bethesda) 2005;20:303-315.
47. Akar FG, Aon MA, Tomaselli GF, et al. The mitochondrial origin of postischemic arrhythmias. J Clin Invest 2005;115(12):3527-3535.
48. Aon MA, O'Rourke B, Cortassa S. The fractal architecture of cytoplasmic organization: scaling, kinetics and emergence in metabolic networks. Mol Cell Biochem 2004;256-257(1-2):169-184.
49. Kleber AG, Rudy Y. Basic mechanisms of cardiac impulse propagation and associated arrhythmias. Physiol Rev 2004;84(2):431-488.
50. Hackenbrock CR. Chemical and physical fixation of isolated mitochondria in low-energy and high-energy states. Proc Natl Acad Sci U S A 1968;61:598-605.
51. Manella CA. The relevance of mitochondrial membrane topology to mitochondrial function. Biochim Biophys Acta 2006;1762:140-147.
52. Manella CA, Pfeiffer DR, Bradshaw PC, et al. Topology of the mitochondrial inner membrane: dynamics and bioenergetic implications. IUBMB Life 2001;52:93-100.
53. Chen H, Chan DC. Critical dependence of neurons on mitochondrial dynamics. Curr Opin Cell Biol 2006;18:453-459.
54. Twig G, Graf SA, Haigh SE, et al. Tagging and tracking individual networks within a complex mitochondrial web with photoactivatable GFP. Am J Physiol Cell Physiol 2006;291:C176-184.
55. Rossignol R, Gilkerson R, Aggeler R, et al. Energy substrate modulates mitochondrial structure and oxidative capacity in cancer cells. Cancer Res 2004;64:985-993.
56. Yi M, Weaver D, Hajnoczky G. Control of mitochondrial motility and distribution by the calcium signal: a homeostatic circuit. J Cell Biol 2004;167:661-672.
57. Anesti V, Scorrano L. The relationship between mitochondrial shape and function and the cytoskeleton. Biochim Biophys Acta 2006;1757:692-699.
58. Aon MA, Cortassa S, Lloyd D. Chaotic dynamics and fractal space in biochemistry: simplicity underlies complexity. Cell Biol Int 2000;24(8):581-587.
59. Aon MA, Roussel MR, Cortassa S, et al. The scale-free dynamics of eukaryotic cells. PLoS ONE 2008;3(11):e3624.
60. Mazloom A, et al. Modeling a Complex Biological Network with Temporal Heterogeneity: Cardiac Myocyte Plasticity as a Case Study. Complex 2009;1(LNICST 4):467-486.
61. Yates FE. Self-organizing systems. In: CAR B, D. N, editors. Oxford: Oxford University Press, 1993:189-218 p.
62. Kuramoto Y. Chemical oscillations, waves, and turbulence. Berlin: Springer-Verlag 1984;
63. Strogatz S. From Kuramoto to Crawford: exploring the onset of synchronization in population of coupled oscillators. Physica D 2000;143:1-20.

64. Strogatz S. The emerging science of spontaneous order. New York: Hyperion books 2003;
65. Winfree A. Biological rhythms and the behavior of populations of coupled oscillators. J Theor Biol 1967;16:15–42.
66. Kesten H. What is ... Percolation? Notices of the American Mathematical Society 2006;53(5):572-573.
67. Bollobás B, Riordan OM. Percolation. Cambridge: Cambridge University Press, 2006.
68. Keller EF. Revisiting "scale-free" networks. BioEssays 2005;27(10):1060-1068.
69. Merton RK. The Matthew effect in science. Science 1968;159:56-63.
70. Aon MA, Cortassa S, O'Rourke B (2007) On the Network Properties of Mitochondria. Molecular System Bioenergetics: Wiley-VCH Verlag GmbH & Co. KGaA. pp. 111-135.
71. Zhou L, O'Rourke B. Cardiac Mitochondrial Network Excitability: Insights from Computational Analysis. American Journal of Physiology - Heart and Circulatory Physiology 2012;
72. Cortassa S, Aon MA, Winslow RL, et al. A mitochondrial oscillator dependent on reactive oxygen species. Biophys J 2004;87(3):2060-2073.
73. Zhou L, Aon MA, Almas T, et al. A Reaction-Diffusion Model of ROS-Induced ROS Release in a Mitochondrial Network. PLoS Comput Biol 2010;6(1):e1000657.
74. Brady NR, Hamacher-Brady A, Westerhoff HV, et al. A wave of reactive oxygen species (ROS)-induced ROS release in a sea of excitable mitochondria. Antioxid Redox Signal 2006;8(9-10):1651-1665.
75. Yang L, Paavo K, Weiss JN, et al. Mitochondrial oscillations and waves in cardiac myocytes: insights from computational models. Biophys J 2010;98:1428-1438.
76. Park J, Lee J, Choi C. Mitochondrial network determines intracellular ROS dynamics and sensitivity to oxidative stress through switching inter-mitochondrial messengers. PLoS ONE 2011;6:e23211.
77. Acebrón JA, Bonilla LL, Vicente P, et al. The Kuramoto model: a simple paradigm for synchronization phenomena. Revies of Modern Physics 2005;77:137-185.
78. Rougemont J, Naef F. Collective synchronization in populations of globally coupled phase oscillators with drifting frequencies. Phys Rev E Stat Nonlin Soft Matter Phys 2006;73(1 Pt 1):011104.
79. Rougemont J, Naef F. Dynamical signatures of cellular fluctuations and oscillator stability in peripheral circadian clocks. Mol Syst Biol 2007;3:93.
80. Uhlenbeck GE, Ornstein LS. On the theory of Brownian motion. Phys Rev 1930;36:823-841.
81. Stanley WC, Recchia FA, Lopaschuk GD. Myocardial substrate metabolism in the normal and failing heart. Physiol Rev 2005;85(3):1093-1129.
82. Han D, Williams E, Cadenas E. Mitochondrial respiratory chain-dependent generation of superoxide anion and its release into the intermembrane space. Biochem J 2001;353(Pt 2):411-416.
83. Slodzinski MK, Aon MA, O'Rourke B. Glutathione oxidation as a trigger of mitochondrial depolarization and oscillation in intact hearts. Journal of Molecular and Cellular Cardiology 2008;45(5):650-660.
84. Backx PH, O'Rourke B, Marban E. Flash photolysis of magnesium-DM-nitrophen in heart cells. A novel approach to probe magnesium- and ATP-dependent regulation of calcium channels. Am J Hypertens 1991;4(7 Pt 2):416S-421S.
85. Mitra R, Morad M. A uniform enzymatic method for dissociation of myocytes from hearts and stomachs of vertebrates. Am J Physiol 1985;249(5 Pt 2):H1056-1060.

86. Backx PH, Gao WD, Azan-Backx MD, et al. Mechanism of force inhibition by 2,3-butanedione monoxime in rat cardiac muscle: roles of [Ca2+]i and cross-bridge kinetics. J Physiol 1994;476(3):487-500.
87. Pavlov AN, Makarov VA, Mosekilde E, et al. Application of wavelet-based tools to study the dynamics of biological processes. Brief Bioinform 2006;7(4):375-389.
88. Refinetti R. Non-stationary time series and the robustness of circadian rhythms. Journal of Theoretical Biology 2004;227(4):571-581.
89. Grossmann A, Morlet J. Decomposition of Hardy Functions into Square Integrable Wavelets of Constant Shape. SIAM Journal on Mathematical Analysis 1984;15(4):723-736.
90. Grossmann A, Morlet J, Paul T. Transforms associated to square integrable group representations. I. General results. Journal of Mathematical Physics 1985;26(10):2473-2479.
91. Walnut DF. An Introduction to Wavelet Analysis. Boston: Birkhäuser Boston, 2001:472 p.
92. Garcia-Ojalvo J, Elowitz MB, Strogatz SH. Modeling a synthetic multicellular clock: repressilators coupled by quorum sensing. Proc Natl Acad Sci U S A 2004;101(30):10955-10960.
93. Suel GM, Garcia-Ojalvo J, Liberman LM, et al. An excitable gene regulatory circuit induces transient cellular differentiation. Nature 2006;440(7083):545-550.
94. Lemons D. An Introduction to Stochastic Processes in Physics. Baltimore and London: The Johns Hopkins University Press, 2002.
95. Hong H, Strogatz SH. Kuramoto model of coupled oscillators with positive and negative coupling parameters: an example of conformist and contrarian oscillators. Phys Rev Lett 2011;106(5):054102.
96. O'Leary DP. Near-optimal parameters for Tikhonov and other regularization methods. SIAM Journal on Scientific Computing 2001;23:1161 - 1171.
97. Park HW, Shin S, Lee HS. Determination of an optimal regularization factor in system identification with Tikhonov regularization for linear elastic continua. International Journal for Numerical Methods in Engineering 2001;51(10):1211-1230.
98. Si BC, Farrell RE. Scale-Dependent Relationship between Wheat Yield and Topographic Indices - A wavelet approach. Soil Science Society of American Journal 2004;68:577-587.
99. Orchard CH, Pasek M, Brette F. The role of mammalian cardiac t-tubules in excitation-contraction coupling: experimental and computational approaches. Exp Physiol 2009;94(5):509-519.
100. Li P, Yi Z. Synchronization of Kuramoto oscillators in random complex networks. Physica A: Statistical Mechanics and its Applications 2008;387(7):1669-1674.
101. Néda Z, Nikitin A, Vicsek T. Synchronization of two-mode stochastic oscillators: a new model for rhythmic applause and much more. Physica A: Statistical Mechanics and its Applications 2003;321(1-2):238-247.
102. Aon MA, Cortassa S, Lloyd D (2011) Chaos in Biochemistry and Physiology. Encyclopedia of Molecular Cell Biology and Molecular Medicine: Wiley-VCH Verlag GmbH & Co. KGaA.
103. Barabasi AL, Oltvai ZN. Network biology: understanding the cell's functional organization. Nat Rev Genet 2004;5(2):101-113.
104. Aon MA, Cortassa S. Dynamic biological organization. Fundamentals as applied to cellular systems. London: Chapman & Hall, 1997.

105. Aon M, Cortassa S, O'Rourke B. Chapter 4: On the network properties of mitochondria. In: Saks V, editor. Weinheim: Wiley-VCH Verlag GmbH & Co. KG, 2007.
106. Mihalcescu I, Hsing W, Leibler S. Resilient circadian oscillator revealed in individual cyanobacteria. Nature 2004;430(6995):81-85.
107. Fang H, Chen M, Ding Y, et al. Imaging superoxide flash and metabolism-coupled mitochondrial permeability transition in living animals. Cell Res 2011;21(9):1295-1304.
108. Lopaschuk GD, Ussher JR, Folmes CDL, et al. Myocardial fatty acid metabolism in health and disease. Physiol Rev 2010;90:207-258.
109. Dimmer KS, Scorrano L. (De)constructing mitochondria: what for? Physiology (Bethesda) 2006;21:233-241.
110. Jezek P, Plecitá-Hlavatá L. Mitochondrial reticulum network dynamics in relation to oxidative stress, redox regulation, and hypoxia. The International Journal of Biochemistry & Cell Biology 2009;41(10):1790-1804.
111. Duchen MR, Leyssens A, Crompton M. Transient mitochondrial depolarizations reflect focal sarcoplasmic reticular calcium release in single rat cardiomyocytes. J Cell Biol 1998;142(4):975-988.
112. Juhaszova M, Zorov DB, Kim SH, et al. Glycogen synthase kinase-3beta mediates convergence of protection signaling to inhibit the mitochondrial permeability transition pore. J Clin Invest 2004;113(11):1535-1549.
113. Afraimovich VS, Verichev NN, Rabinovich MI. Izv Vyssh Uchebn Zaved, Radiofiz 1986;29:1050.
114. Fujisaka H, Yamada T. Prog Theor Phys 1983;69:32.
115. Pecora LM, Carroll TL. Phys Rev Lett 1990;64:821.
116. Belykh VN, Osipov GV, Petrov VS, et al. Cluster synchronization in oscillatory networks. CHAOS 2008;18:037106.
117. Wang X, Zhou C, Lai CH. Multiple effects of gradient coupling on network synchronization. Physical Review E 2008;77(5):056208.056201-056205.
118. Aon MA, Cortassa S, Maack C, et al. Sequential opening of mitochondrial ion channels as a function of glutathione redox thiol status. J Biol Chem 2007;282(30):21889-21900.
119. Bassenge E, Sommer O, Schwemmer M, et al. Antioxidant pyruvate inhibits cardiac formation of reactive oxygen species through changes in redox state. Am J Physiol Heart Circ Physiol 2000;279(5):H2431-2438.
120. Stanley WC. Changes in cardiac metabolism: a critical step from stable angina to ischaemic cardiomyopathy. European Heart Journal Supplements 2001;O:O2-O7.
121. Kembro JM, Aon MA, Winslow RL, et al. Integrating mitochondrial energetics, redox and ROS metabolic networks: a two-compartment model. Biophys J 104(2):332-343.
122. Chatham JC, Gao ZP, Bonen A, et al. Preferential inhibition of lactate oxidation relative to glucose oxidation in the rat heart following diabetes. Cardiovasc Res 1999;43(1):96-106.
123. Chatham JC, Gao ZP, Forder JR. Impact of 1 wk of diabetes on the regulation of myocardial carbohydrate and fatty acid oxidation. Am J Physiol 1999;277(2 Pt 1):E342-351.
124. Jeffrey FM, Diczku V, Sherry AD, et al. Substrate selection in the isolated working rat heart: effects of reperfusion, afterload, and concentration. Basic Res Cardiol 1995;90(5):388-396.

125. Hashimoto T, Hussien R, Oommen S, et al. Lactate sensitive transcription factor network in L6 cells: activation of MCT1 and mitochondrial biogenesis. Faseb J 2007;21(10):2602-2612.
126. Aon MA, Cortassa S, O'Rourke B. Is there a mitochondrial clock? In: Lloyd D, Rossi EL, editors. New York Springer-Verlag, 2008.
127. Murray DB, Roller S, Kuriyama H, et al. Clock control of ultradian respiratory oscillation found during yeast continuous culture. J Bacteriol 2001;183(24):7253-7259.
128. Murphy MP. How mitochondria produce reactive oxygen species. Biochem J 2009;417(Pt 1):1-13.

VI. Eidesstattliche Versicherung

„Ich, Felix Tobias Kurz, versichere an Eides statt durch meine eigenhändige Unterschrift, dass ich die vorgelegte Dissertation mit dem Thema: “Network dynamics of coupled mitochondrial oscillators in cardiac cells” selbstständig und ohne nicht offengelegte Hilfe Dritter verfasst und keine anderen als die angegebenen Quellen und Hilfsmittel genutzt habe.

Alle Stellen, die wörtlich oder dem Sinne nach auf Publikationen oder Vorträgen anderer Autoren beruhen, sind als solche in korrekter Zitierung (siehe „Uniform Requirements for Manuscripts (URM)“ des ICMJE -*www.**icmje**.org*) kenntlich gemacht. Die Abschnitte zu Methodik (insbesondere praktische Arbeiten, Laborbestimmungen, statistische Aufarbeitung) und Resultaten (insbesondere Abbildungen, Graphiken und Tabellen) entsprechen den URM (s.o) und werden von mir verantwortet.

Meine Anteile an den ausgewählten Publikationen entsprechen denen, die in der untenstehenden gemeinsamen Erklärung mit dem/der Betreuer/in, angegeben sind. Sämtliche Publikationen, die aus dieser Dissertation hervorgegangen sind und bei denen ich Autor bin, entsprechen den URM (s.o) und werden von mir verantwortet.
Die Bedeutung dieser eidesstattlichen Versicherung und die strafrechtlichen Folgen einer unwahren eidesstattlichen Versicherung (§156,161 des Strafgesetzbuches) sind mir bekannt und bewusst.

_____

Datum Unterschrift

VII. Anteilserklärung an bisher erfolgten und zu erfolgenden Publikationen

Felix Kurz hatte folgenden Anteil an den folgenden Publikationen:

Publikation 1: Kurz FT, Aon MA, O'Rourke B, Armoundas AA, *Wavelet analysis reveals heterogeneous time-dependent oscillationsof individual mitochondria,* American Journal of Physiology: Heart and Circulatory Physiology, 2010

Beitrag im Einzelnen:

Durchführung der zugrundeliegenden Experimente, Datenanalyse der Experimente, Entwicklung der beschriebenen Analyse- und Signalprozessierungsprogramme, Verfassen des Artikels

Publikation 2: Kurz FT, Aon MA, O'Rourke B, Armoundas AA, *Spatio-temporal oscillations of individual mitochondria in cardiac myocytes reveal modulation of synchronized mitochondrial clusters*, Proceedings of the National Academy of Sciences, USA, 2010

Beitrag im Einzelnen:

Durchführung der zugrundeliegenden Experimente, Datenanalyse der Experimente, Entwicklung der beschriebenen Analyse- und Signalprozessierungsprogramme, Verfassen des Artikels

Publikation 3 (in Vorbereitung): Kurz FT, Derungs T, Aon MA, O'Rourke B, Armoundas AA, *Mitochondrial networks in cardiac myocytes reveal dynamic coupling behavior.*

Beitrag im Einzelnen:

Durchführung der zugrundeliegenden Experimente, Datenanalyse der Experimente, Entwicklung der beschriebenen Analyse- und Signalprozessierungsprogramme, Verfassen des Artikels

Datum _____ Unterschrift

VIII. Curriculum Vitae Felix Tobias Kurz

Mein Lebenslauf wird aus datenschutzrechtlichen Gründen in der elektronischen Version meiner Arbeit nicht veröffentlicht.

IX. Publikationsliste

1) **Autoren:** Kurz, Felix T.,
Aon, Miguel A.,
O'Rourke, Brian
Armoundas, Antonis A.

Titel: Wavelet analysis reveals heterogeneous time-dependent oscillations of individual mitochondria

Journal: American Journal of Physiology: Heart and Circulatory Physiology
Volume 299, Issue 5, pages: H1736–H1740.

Datum: November 2010

2) **Autoren:** Kurz, Felix T.,
Aon, Miguel A.,
O'Rourke, Brian
Armoundas, Antonis A.

Titel: Spatio-temporal oscillations of individual mitochondria in cardiac myocytes reveal modulation of synchronized mitochondrial clusters

Journal: Proceedings of the National Academy of Sciences, USA
Volume 107, Issue 32, pages: 14315–14320.

Datum: August 2010

X. Danksagung

Mein Dank gilt insbesondere Herrn Professor Antonis Armoundas. Herr Armoundas hat mich sehr herzlich in sein Labor in Boston aufgenommen und hat mich mit großem zeitlichen Aufwand in die Thematik eingearbeitet. Bei Problemen und Fragestellungen konnte er mir durch ausführliche Diskussionen meist die richtigen Denkanstöße geben. Ich habe mich in seinem Labor sehr wohl gefühlt und blicke voller Dankbarkeit auf unsere Zusammenarbeit in den letzten Jahren zurück.

Weiter gilt mein Dank meinem Doktorvater Herrn PD Cemil Özcelik, der mich stets bedingungslos unterstützt hat und ohne den diese Arbeit nicht möglich gewesen wäre.

Auch möchte ich Herrn Professor Brian O'Rourke, Herrn Professor Miguel Aon sowie Frau Professor Sonia Cortassa für die Unterstützung meiner Arbeit danken. Während meines Aufenthaltes in Baltimore haben mir Brian, Miguel und Sonia wertvolle Ideen für mein Projekt und spannende Einblicke in ihre Arbeit geben können.

Mein weiterer Dank gilt meinen Laborkollegen Thomas Derungs, Victoria Heller und Eric Weiss, sowie Dr. Dheeraj Puppala und Dr. Faisal Merchant für ihre tatkräftige Unterstützung. Herrn Dr. Christian Geier danke ich für seine freundschaftlichen Ratschläge und Hilfeleistungen.

Ganz besonders danke ich der Stiftung für medizinische Grundlagenforschung des Böhringer-Ingelheim-Fonds für die großzügige finanzielle Unterstützung.

Außerdem und abschließend will ich meiner Mutter Ingrid, meinem Vater Karlheinz und meinem Bruder Patrick danken für die moralische Unterstützung.